NASA/TM-20205009045

NASA Glenn Icing Research Tunnel: 2019 Cloud Calibration Procedure and Results

Emily N. Timko
Jacobs Technology, Cleveland, Ohio

Laura E. King-Steen
HX5 Sierra, LLC, Cleveland, Ohio

Judith F. Van Zante and Waldo J. Acosta
Glenn Research Center, Cleveland, Ohio

December 2021

NASA STI Program . . . in Profile

Since its founding, NASA has been dedicated to the advancement of aeronautics and space science. The NASA Scientific and Technical Information (STI) Program plays a key part in helping NASA maintain this important role.

The NASA STI Program operates under the auspices of the Agency Chief Information Officer. It collects, organizes, provides for archiving, and disseminates NASA's STI. The NASA STI Program provides access to the NASA Technical Report Server—Registered (NTRS Reg) and NASA Technical Report Server—Public (NTRS) thus providing one of the largest collections of aeronautical and space science STI in the world. Results are published in both non-NASA channels and by NASA in the NASA STI Report Series, which includes the following report types:

- TECHNICAL PUBLICATION. Reports of completed research or a major significant phase of research that present the results of NASA programs and include extensive data or theoretical analysis. Includes compilations of significant scientific and technical data and information deemed to be of continuing reference value. NASA counter-part of peer-reviewed formal professional papers, but has less stringent limitations on manuscript length and extent of graphic presentations.

- TECHNICAL MEMORANDUM. Scientific and technical findings that are preliminary or of specialized interest, e.g., "quick-release" reports, working papers, and bibliographies that contain minimal annotation. Does not contain extensive analysis.

- CONTRACTOR REPORT. Scientific and technical findings by NASA-sponsored contractors and grantees.

- CONFERENCE PUBLICATION. Collected papers from scientific and technical conferences, symposia, seminars, or other meetings sponsored or co-sponsored by NASA.

- SPECIAL PUBLICATION. Scientific, technical, or historical information from NASA programs, projects, and missions, often concerned with subjects having substantial public interest.

- TECHNICAL TRANSLATION. English-language translations of foreign scientific and technical material pertinent to NASA's mission.

For more information about the NASA STI program, see the following:

- Access the NASA STI program home page at http://www.sti.nasa.gov

- E-mail your question to help@sti.nasa.gov

- Fax your question to the NASA STI Information Desk at 757-864-6500

- Telephone the NASA STI Information Desk at 757-864-9658

- Write to:
  NASA STI Program
  Mail Stop 148
  NASA Langley Research Center
  Hampton, VA 23681-2199

NASA/TM-20205009045

NASA Glenn Icing Research Tunnel: 2019 Cloud Calibration Procedure and Results

Emily N. Timko
Jacobs Technology, Cleveland, Ohio

Laura E. King-Steen
HX5 Sierra, LLC, Cleveland, Ohio

Judith F. Van Zante and Waldo J. Acosta
Glenn Research Center, Cleveland, Ohio

National Aeronautics and
Space Administration

Glenn Research Center
Cleveland, Ohio 44135

December 2021

Acknowledgments

The authors would like to thank NASA's Aerosciences Evaluation and Test Capabilities (AETC) Project for funding this cloud calibration effort. The Icing Research Tunnel (IRT) engineering staff also provided support with cloud calibration efforts and the authors would like to acknowledge those individuals. The cloud calibration could not have been successful without the important work done by the IRT technician staff, as well. Special thanks to Robert Ide for his continued guidance on IRT cloud principles and operations.

Level of Review: This material has been technically reviewed by technical management.

Available from

NASA STI Program
Mail Stop 148
NASA Langley Research Center
Hampton, VA 23681-2199

National Technical Information Service
5285 Port Royal Road
Springfield, VA 22161
703-605-6000

This report is available in electronic form at http://www.sti.nasa.gov/ and http://ntrs.nasa.gov/

NASA Glenn Icing Research Tunnel: 2019 Cloud Calibration Procedure and Results

Emily N. Timko
Jacobs Technology
Cleveland, Ohio 44135

Laura E. King-Steen
HX5 Sierra, LLC
Cleveland, Ohio 44135

Judith F. Van Zante and Waldo J. Acosta
National Aeronautics and Space Administration
Glenn Research Center
Cleveland, Ohio 44135

Summary

The NASA Glenn Research Center 2019 Icing Research Tunnel cloud calibration results are presented in this report. The current status of the cloud uniformity, liquid water content, and drop-size calibration results will be discussed. The goals achieved in this calibration were to establish a uniform cloud and to generate transfer functions from the inputs of airspeed, spray bar atomizing air pressure, and spray bar water pressure to the outputs of median volumetric diameter (drop-size distributions) and liquid water content. This was completed for both Federal Aviation Administration (FAA) 14 CFR Parts 25 and 29, Appendix C ("typical" icing) and Appendix O (supercooled large drop) conditions. The cloud uniformity from the Standard nozzles has remained the same as that reported for the 2014 full calibration. Changes were made to the Mod1 nozzle cloud, resulting in higher liquid water content values associated with the Mod1 cloud.

Nomenclature

CDP	Cloud Droplet Probe, drop sizer, 2 to 50 μm
DMT	Droplet Measurement Technologies
$D_{v0.n}$	drop diameter at which n percent of the total volume of water is contained in smaller drops
FAA	Federal Aviation Administration
FZDZ	Freezing Drizzle
FZRA	Freezing Rain
IRT	Icing Research Tunnel
K	function of V and P_{air}
LWC	liquid water content, g/m^3
MVD	median volumetric diameter, μm
OAP–230X	Optical Array Probe, drop sizer, 15 to 450 μm
OAP–230Y	Optical Array Probe, drop sizer, 50 to 1,500 μm

P_{air}	spray nozzle atomizing air pressure, psig
P_{water}	spray nozzle water pressure, psig
RTD	resistance temperature detector
SEA, Inc.	Science Engineering Associates, Inc.
SLD	supercooled large drop conditions in the IRT: Mod1 nozzles, $2 \le P_{air} \le 8$ psig
Std	standard
TWC	total water content, g/m^3
V	calibrated true airspeed (velocity) in the test section, kn
ΔP	spray nozzle $P_{water} - P_{air}$, psid

1.0 Introduction

The NASA Glenn Icing Research Tunnel (IRT) completed a full icing cloud calibration between February and May 2019 in accordance with the guidelines of SAE Aerospace Recommended Practice ARP5905, "Calibration and Acceptance of Icing Wind Tunnels" (Ref. 1). SAE ARP5905 recommends that a full calibration be performed 5 years following the previous full calibration, and the last full calibration of the IRT cloud was completed in 2014 and 2015 (Ref. 2). This report covers the procedures and results from the 2019 IRT full cloud calibration.

The steps taken to perform the calibration included establishing a uniform cloud and completing drop-size and liquid water content (LWC) calibrations for both Federal Aviation Administration (FAA) 14 CFR Parts 25 and 29, Appendix C ("typical" icing) and Appendix O (supercooled large drop, SLD) conditions (Refs. 3 and 4). The first goal achieved of the calibration was to develop a uniform cloud for each nozzle set of the facility, Mod1 and Standard nozzles. Nozzle spraying locations were optimized; the number of spraying Mod1 nozzles increased to 103 and the Standard nozzle map remained the same at 165 nozzles. Another goal was to generate transfer functions from the inputs of airspeed, spray bar atomizing air pressure, and spray bar water pressure to the outputs of median volumetric diameter (MVD) and LWC. New MVD and LWC curve fits for both the Mod1 and Standard nozzle sets were developed using the acquired data. The curves fit the data within ±10 percent for the Appendix C icing criteria and ±20 percent for the SLD Appendix O icing conditions.

The IRT engineers find it necessary to report that the check calibrations completed in 2020 indicated that most of the cloud parameters were within expected repeatability tolerance but a small section of the operating envelopes (air pressure P_{air} setting ≥10 psig and $\Delta P \le 10$ psid) were found to be 12 to 24 percent low and outside the stated ±10 percent calibration limits. The cause for this change is under investigation but has not been determined at the time of this writing. Modifying the curve fit equations might be necessary and the staff expect to address the problem and take additional data to investigate.

2.0 Facility Description

The IRT is a closed-loop refrigerated wind tunnel that simulates flight through an icing cloud. Figure 1 shows a plan view of the facility. A 5,000-hp (3,728.5-kW) motor drives the 24-ft- (7.3-m-) diameter fan with blades made of wood from Sitka spruce. The fan drives air through expanding turning vanes in the C corner (see Figure 1) and into the face of the staggered 26-ft- (7.9-m-) high, 50-ft- (15.2-m-) wide heat exchanger. There, the air is chilled or warmed within a temperature range of 15 °C (59 °F) total to –35 °C (–31 °F) static. Twenty-four resistance temperature detectors, RTDs, are distributed on the D corner contracting turning vanes and measure the total temperature in the settling chamber.

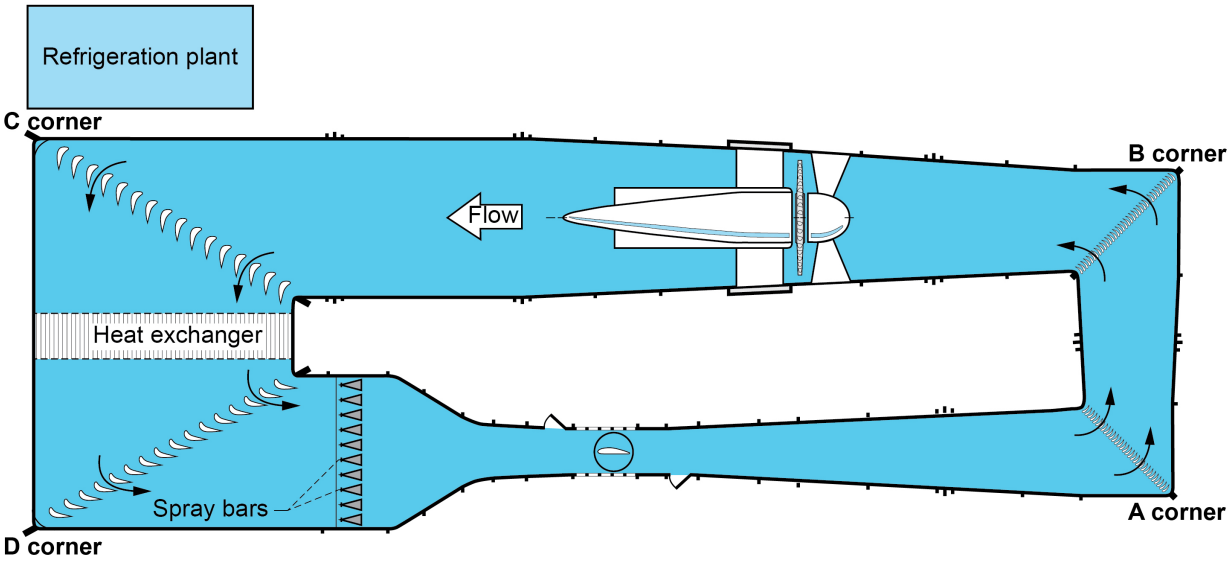

Figure 1.—NASA Glenn Research Center Icing Research Tunnel.

Downstream of the D corner contracting turning vanes are 10 spray bars with two different air-atomizing nozzle types: Mod1 and Standard. The Mod1 nozzles have a lower water flow rate than the Standard nozzles. Each bar has 55 nozzle positions that contain either a Mod1 nozzle, a Standard nozzle, or a plug. The nozzle housings are connected to an air manifold and two water manifolds. The cloud (spray) is turned on using remotely controlled solenoid valves. The water manifolds can be individually turned on to spray only the Mod1 nozzles, only the Standard nozzles, or both (with the same atomizing air pressure). In 2006, vertically mounted struts were added to the spray bars. These struts were installed to improve the cloud uniformity and are still part of the system (Ref. 5).

The contraction area ratio into the test section is 14:1. The test section itself is 20 ft (6.1 m) long (axial) by 6 ft (1.8 m) high by 9 ft (2.7 m) wide. The center of the test section is 44 ft (13.4 m) from the spray bars. From the test section, the cloud flows into the diffuser toward A corner, into B corner, and into the fan. The calibrated speed range in the test section is from 50 to 300 kn.

3.0 Icing Cloud Uniformity

The first step in the calibration process was to establish a uniform cloud. This was done by optimizing a spray nozzle pattern that has the appropriate nozzles turned on or off for both the Mod1 and Standard nozzle sets to produce a uniform cloud.

Figure 2(a) shows the grid that was used to measure the cloud uniformity. The grid is 6 ft (1.8 m) high by 6 ft (1.8 m) wide and extends from the floor to the ceiling of the test section. The mesh elements are 2 in. (5.08 cm) deep with a flat 0.125-in. (0.3175-cm) face for ice accretion. Ice is accreted across the grid and then accretion thicknesses are measured on the vertical mesh elements, which are spaced every 6 in. (15.24 cm). Digital calipers are used to measure the ice thickness at the center point of the vertical elements. Figure 2(b) is an example of the accreted ice on the grid. The measured accretion values are then plotted as a ratio of the average of the central 12 values. Examples are shown in Figure 3. The light green color shows that the LWC uniformity is within ±10 percent for most of the map.

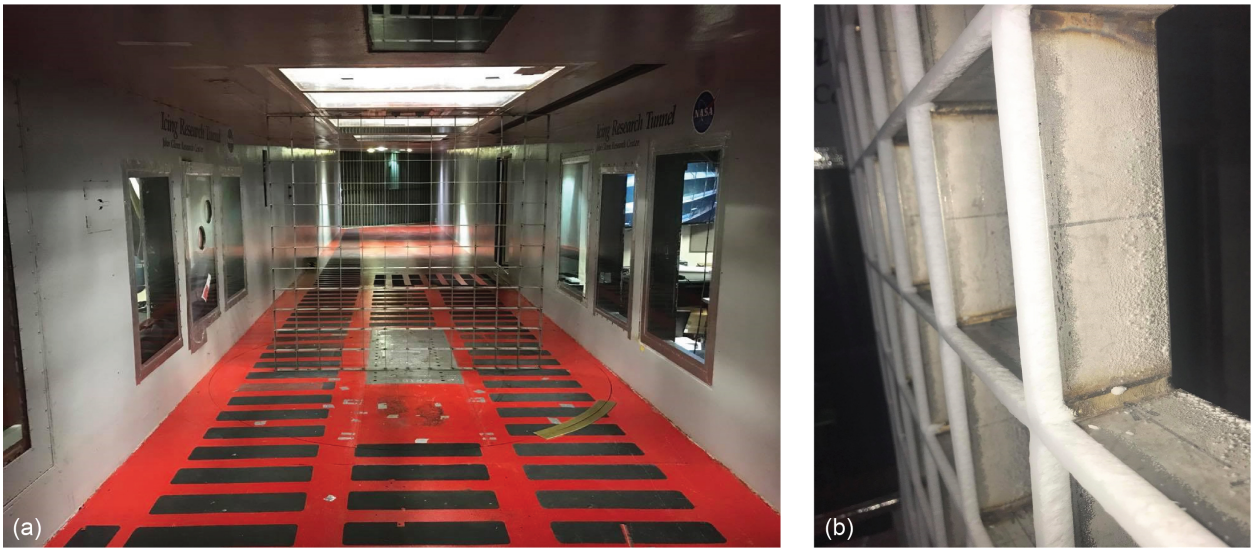

Figure 2.—Cloud uniformity grid. (a) Grid mounted in center of test section in Icing Research Tunnel. (b) Ice accretion on grid elements.

A nozzle transfer map was established as a primary step in developing a uniform cloud. Single rows (i.e., spray bars) and columns of nozzles were sprayed to observe where ice accretes on the grid. This transfer map aids in the optimization of nozzle locations to produce a uniform cloud. Nozzle transfer maps can also be used as a tool to identify problematic nozzles during routine testing. In accordance with ARP5905 (Ref. 1), the IRT performed semiannual check calibrations between the 2014 full calibration and the 2019 full calibration. During this timeframe, there were no changes to the facility or the Standard or Mod1 nozzle spray patterns. From the check calibrations it was observed that the Standard nozzle cloud uniformity (created by 165 spraying nozzles) remained generally unchanged over the 5 years. Hence, in 2019, the Standard nozzle map was not altered, and it still contains 165 spraying nozzles. The Mod1 cloud uniformity (created by 88 spraying nozzles) remained within ARP5905 recommendations but it had become less uniform by July 2018. It was assumed that increasing the total number of Mod1 nozzles would make the Mod1 nozzle uniformity more robust because the uniformity for Standard nozzles remained unchanged with a nozzle pattern containing 165 nozzles. Therefore, 15 spraying nozzles were added to the Mod1 nozzle map resulting in a total of 103 spraying nozzles. The resulting cloud uniformity maps are shown in Figure 3(a) and (b) for Mod1 nozzles and Standard nozzles, respectively. These plots are viewed facing downstream. The additional Mod1 spray nozzles resulted in an increase in the IRT's Mod1 LWC values, which can be observed in the operating envelopes near the end of this report. Uniformity for an SLD case, MVD = 129 μm, is shown in Figure 3(c). The vertical extent of the cloud is smaller than those in the aforementioned figures, but this was foreseen due to expected drop trajectories of larger sized drops.

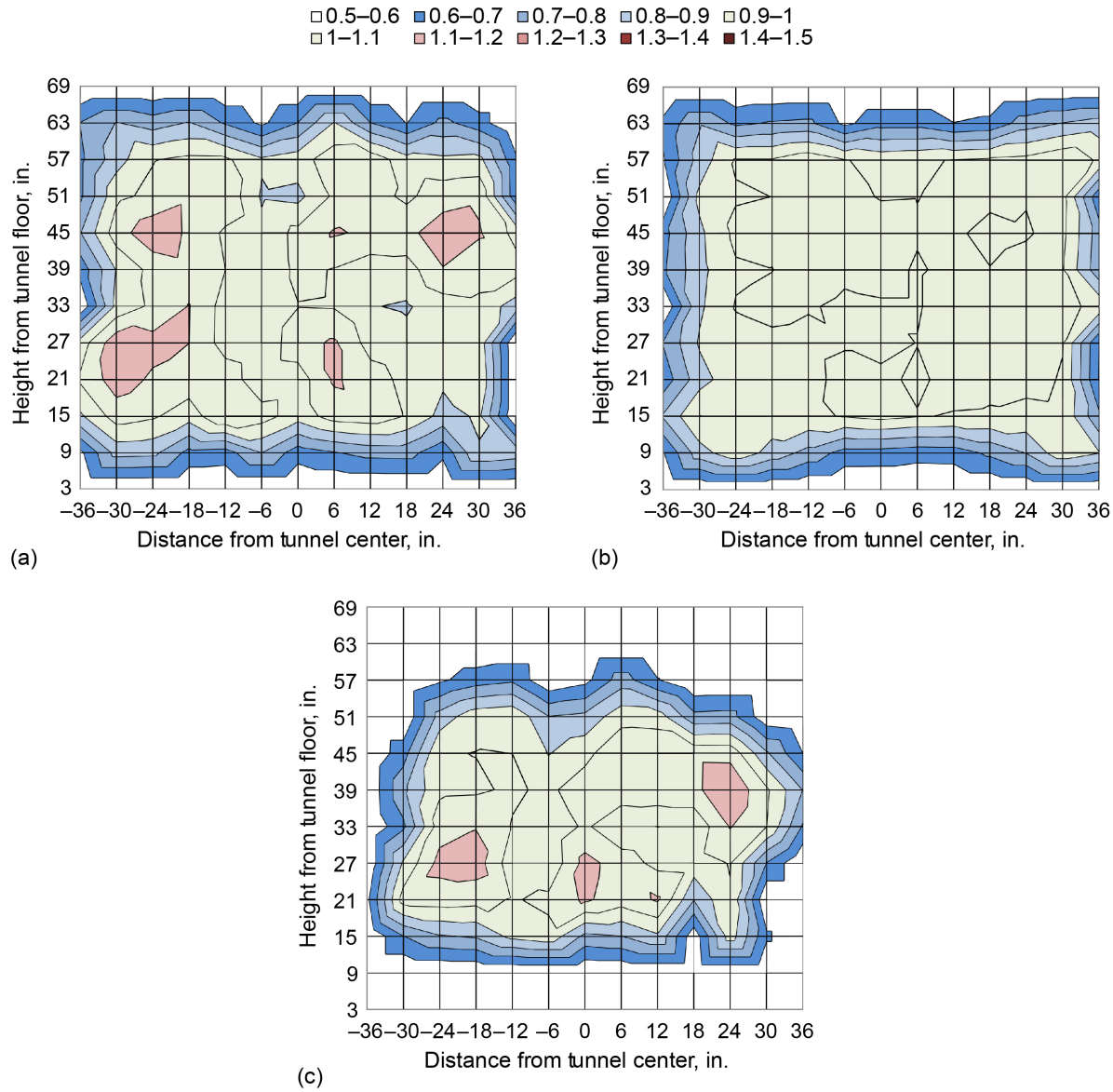

Figure 3.—Cloud uniformity viewed facing downstream, plotted as ratios to average accretion thickness from center 12 elements. (a) Mod1 nozzle cloud uniformity, 20-μm median volumetric diameter (MVD) at an airspeed of 150 kn. (b) Standard nozzle cloud uniformity, 20-μm MVD at an airspeed of 150 kn. (c) Supercooled large drop cloud uniformity, 129-μm MVD at an airspeed of 150 kn.

4.0 Drop-Size Calibration

Following the development of the cloud uniformity, a complete set of drop-size data was collected. In order to measure the full range of drop sizes in the IRT, three instruments were needed. For the 2019 drop-size calibration, the instruments used were the Cloud Droplet Probe (CDP) made by Droplet Measurement Technologies (DMT) and two Optical Array Probes (OAP–230X and OAP–230Y) made by Particle Measuring Systems. Figure 4 shows these probes mounted in the IRT test section.

The CDP measures drop sizes between 2 to 50 μm in diameter using the Mie-scattering theory for forward-scattered light intensity. When a drop passes through the beam path of the CDP laser, it scatters light in all directions and the forward-scattered light intensity is recorded by the probe and used to sort the drop size into one of 30 size bins or ranges. Since the CDP measures the smallest drop sizes of the three probes and since all spray conditions in the IRT contain small drops, data from the CDP is collected and used for the full range of spray conditions. The range of the spray conditions covered the following air pressures (P_{air}) and delta pressures (ΔP equals water pressure, P_{water}, minus P_{air} or $\Delta P = P_{water} - P_{air}$); for the nozzles, Mod1 are at $2 \le P_{air} \le 60$ psig and $5 \le \Delta P \le 250$ psid and Standard are at $10 \le P_{air} \le 60$ psig and $5 \le \Delta P \le 150$ psid.

The OAP–230X measures drop sizes between 15 to 450 μm and the OAP–230Y measures between the range of 50 to 1,500 μm. Both of the optical array probes measure drop size using diode shadowing. An array of photodiodes is illuminated by a collimated laser beam and when a drop passes through the beam, the drop diameter is sorted into bins according to the number of diodes that are shadowed by more than 50 percent. At least one diode must be shadowed by 66 percent for the particle to be counted. Data were taken with the OAP–230X for all spray conditions that produce an MVD greater than 15 μm. The OAP–230Y usage was limited to larger drop conditions, that is, spray conditions that produced an MVD above 50 μm. Drop-size distributions were determined by combining data from the CDP with the OAP–230X and OAP–230Y to calculate MVD.

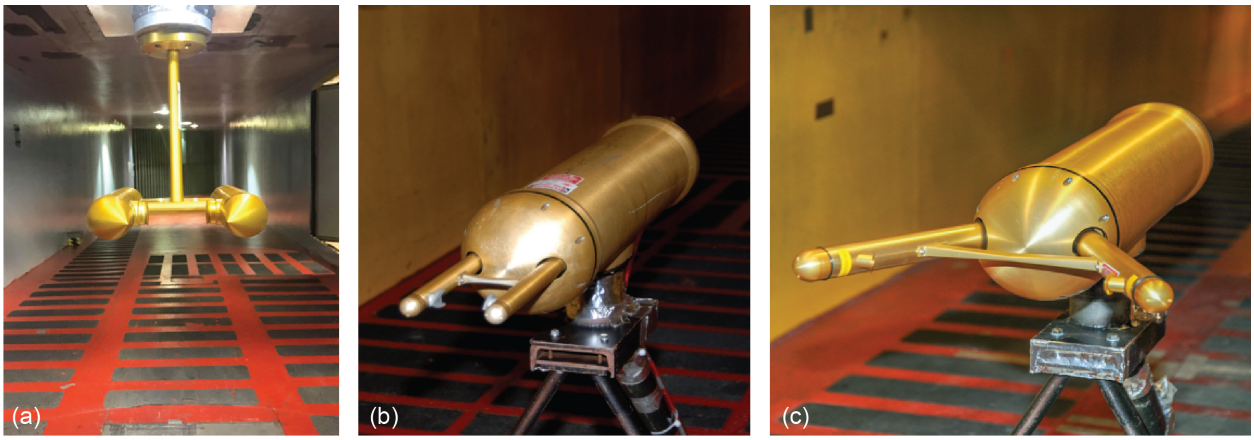

Figure 4.—Three drop sizing instruments used for drop-size calibration mounted in Icing Research Tunnel test section. (a) Cloud Droplet Probe (CDP) by Droplet Measurement Technologies, 2 to 50 μm. (b) Optical Array Probe (OAP–230X), 15 to 450 μm and (c) Optical Array Probe (OAP–230Y), 50 to 1,500 μm are both made by Particle Measuring Systems.

4.1 Data Processing of Drop-Size Distributions

An example drop-size distribution is shown in Figure 5 combining all three probes for an SLD spray condition. The number density is the number of drops that are recorded in each bin normalized by the sample volume for that drop size and the bin width. For Figure 5(a) and (b), the squares show the size distribution as measured by the CDP, the triangles by the OAP–230X, and the circles by the OAP–230Y. The gray data points represent measurements from the respective probes that were not used in MVD calculation, as will be described in the following information. The volume is calculated using the median bin diameter size multiplied by the number of recorded counts, which then results in the LWC for each bin. Figure 5(b) shows an example LWC distribution for a case with an MVD of 223 μm where values are normalized by their respective bin widths. The MVD can then be determined by plotting the normalized cumulative water content versus drop diameter, as seen in Figure 5(c). Drop-size distributions are characterized by the MVD. This is the value at which half of the water volume is contained in smaller (or larger) drops. MVD can also be referred to as "$D_{v0.50}$". Correspondingly, $D_{v0.90}$ is the diameter at which 90 percent of the volume is contained in smaller drops. Normalized cumulative volume distributions for the IRT are shown in Figure 6. Bin volumes are plotted cumulatively, such that each data point represents the amount of water contained in all smaller diameters normalized by the total volume contained in all bins. Figure 6(a) shows cumulative volume distributions for MVD values less than or equal to 50 μm, and Figure 6(b) shows cumulative volume distributions for MVD greater than 50 μm.

As noted, the CDP, OAP–230X, and OAP–230Y each contribute measurements to the overall particle size distribution based on their sizing ranges. Their size ranges overlap, and efforts were made to determine how to address that overlap. A change for this calibration was to cross over from the CDP to the OAP number densities at 46 μm, instead of 50 μm used previously. For the 2019 full calibration, IRT staff chose to not use the uppermost bins from the CDP or the OAP–230X if there were accompanying data from the larger size range probe. For the CDP, this was because the two uppermost bins (size range 46 to 50 μm) did not always follow the expected trend and often increased in number density as diameter increased. This can be observed in Figure 5(a) and (b) with two gray squares just below 50 μm. This was observed consistently in these two bins and tended to be more pronounced when large particles (which cannot be sized by the CDP) were present in the spray. In 2015, this behavior was observed for only one condition. It is expected to be an instrumentation error, though the cause is yet unknown. It is not likely to be a probe alignment issue because this behavior was observed even when the probe was newly received after realignment at DMT in 2017. Since the CDP otherwise shows good alignment with the OAP–230X measurements, the choice was made to use CDP data for diameters up to 46 μm and then use the OAP–230X data.

For the 2019 full calibration data, it was decided to use the OAP–230X for particle sizes up to 367.5 μm and then use (crossover) OAP–230Y data if it were available. This diameter value was chosen because it was the most common value at which the OAP–230X was observed to deviate from the trend that was continued by the OAP–230Y as observed in Figure 5(b). Similar to the decision for CDP and OAP–230X crossover data, the uppermost bins from the OAP–230X were not used if there was OAP–230Y data that could be used instead. This is because the OAP–230Y showed good agreement with the overall trend of the distribution, while the uppermost bins of the OAP–230X appear to be undercounting, as can be seen by the gray triangles in Figure 5(b). Both OAPs only return one-dimensional (1D) data, and if a particle shadows either end (qualifier) diode, it is not sized, and thus it becomes statistically difficult for particles at the upper end of the probe's range to pass through the middle of the sizing array. Hence, these particles may be undercounted. It should be noted that for both the CDP and OAP–230X, these issues become more pronounced as MVD increased, and it was not generally necessary to discard probe data at these values if no larger range data was taken.

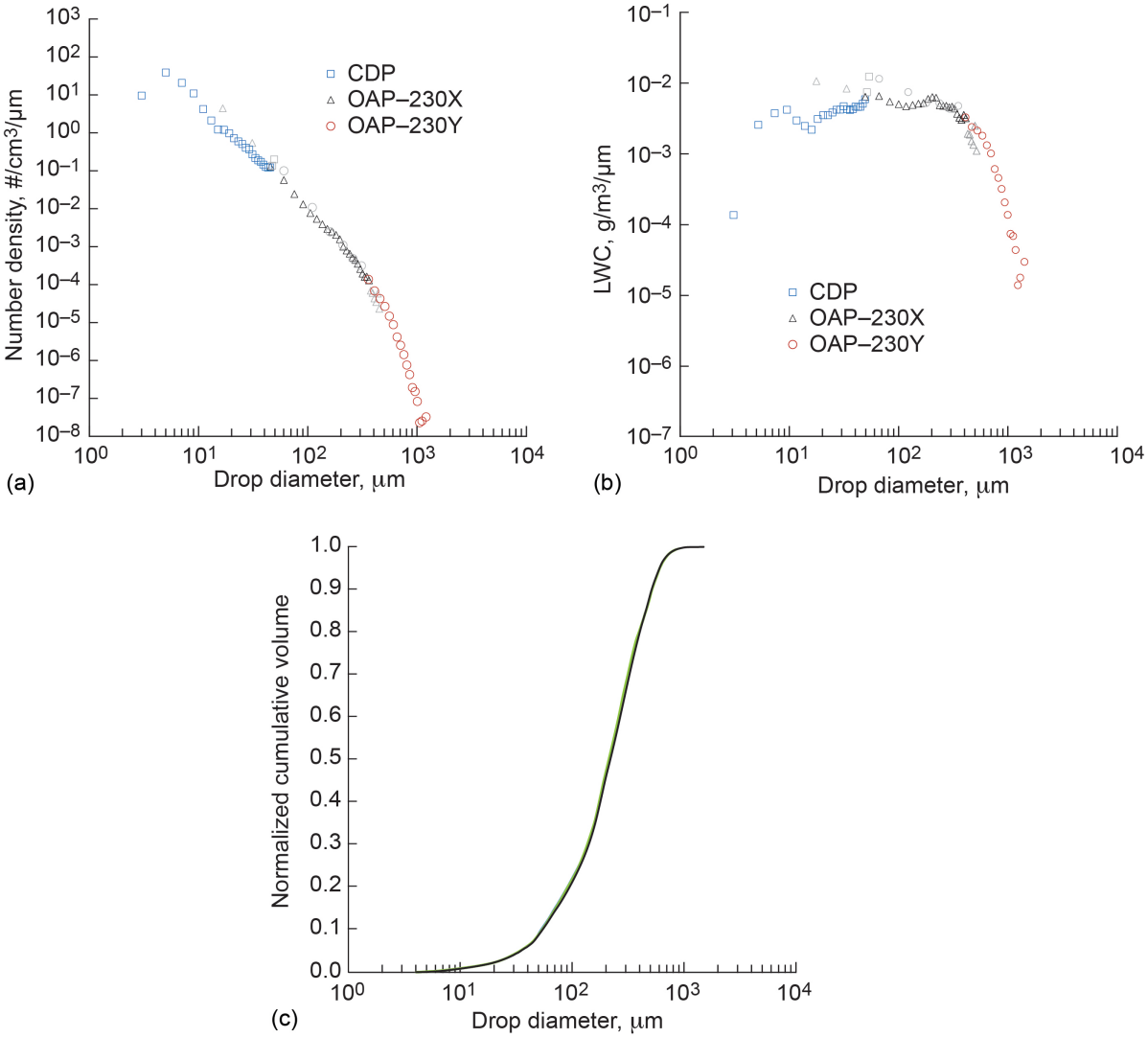

Figure 5.—Drop-size distribution combining all three probes for median volumetric diameter (MVD) = 223 μm including the number density distribution, cumulative volume distribution, and the liquid water content (LWC) distribution. All go into calculations for MVD. Gray data points represent measurements from respective probes that were not used in MVD calculation. (a) Number density distribution. (b) LWC distribution. (c) Cumulative volume distribution.

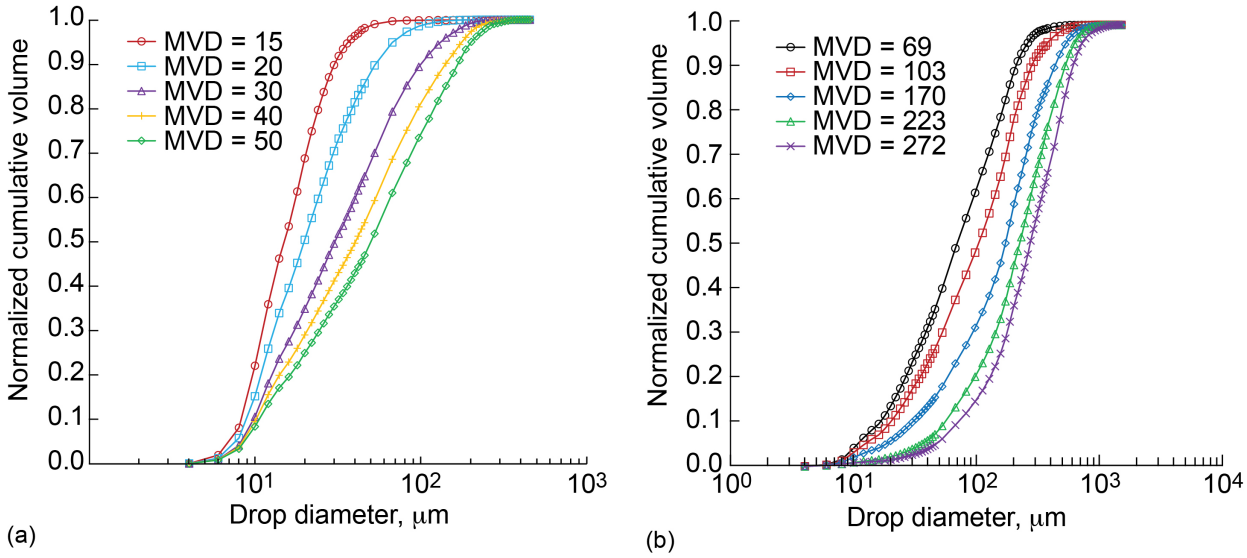

Figure 6.—Normalized cumulative volume plots for two Icing Research Tunnel drop size regimes. (a) Size range 15 to 50 μm. (b) Size range >50 μm up to maximum calibrated. Median volumetric diameter (MVD).

4.2 Drop-Size Equations

The purpose of the drop-size calibration is not only to determine drop-size distributions but also to develop curve fit equations. The equations developed have an input of measured atomizing P_{air} and ΔP ($P_{water} - P_{air}$). The curve fit generator, TableCurve 3D (Systat Software, Inc.) was used to generate an appropriate equation that fit the majority of the data within ±10 percent.

The Mod1 MVD curve fit equation is

$$\mathrm{MVD}_{\mathrm{Mod1}} = a + bP_{\mathrm{air}}^{c} + d\Delta P^{e} + fP_{\mathrm{air}}^{c}\Delta P^{e} \tag{1}$$

where a = 10.9129312, b = 350.904404, c = –2.408871, d = 0.00017583, e = 1.57507361, and f = 21.9700778.

The Standard MVD curve fit equation is

$$\mathrm{MVD}_{\mathrm{Standards}} = a + b\left[\frac{1}{1+\left(\frac{P_{\mathrm{air}}}{c}\right)^{-d}}\right] + e\left[\frac{1}{1+\left(\frac{\Delta P}{f}\right)^{-g}}\right] + h\left[\frac{1}{1+\left(\frac{P_{\mathrm{air}}}{c}\right)^{-d}}\right] * \left[\frac{1}{1+\left(\frac{\Delta P}{f}\right)^{-g}}\right] \tag{2}$$

where a = 16.9540224, b = –3.1943582, c = 9.46677487, d = 3.50333948, e = 145,572.653, f = 380.990642, g = 2.35580256, and h = –145,519.81.

Figure 7(a) and (b) summarize these curve fits for Mod1 and Standard nozzles, respectively. In Figure 7, the curve fit lines are plotted as a function of ΔP for each calibrated P_{air} line. Measured MVDs are plotted against the respective curve fits for two P_{air} lines in each plot. Figure 8(a) and (b) show how the curve fit values from the generated equations compare to the measured values for all Mod1 and Standard conditions, respectively. These plots show that the curve fits for the data points are within the IRT's typical targeted accuracy of ±10 percent.

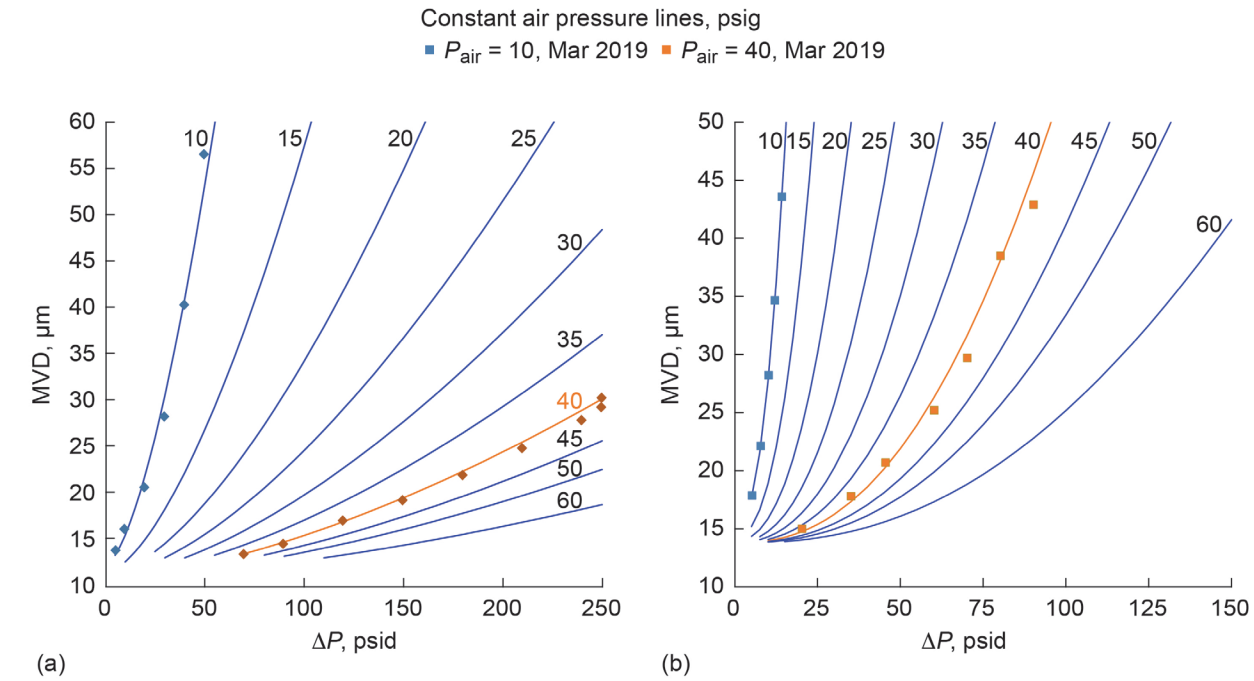

Figure 7.—Median volumetric diameter (MVD) curve fits as function of ΔP for each atomizing air pressure (P_{air}). (a) Mod1 nozzles. (b) Standard nozzles.

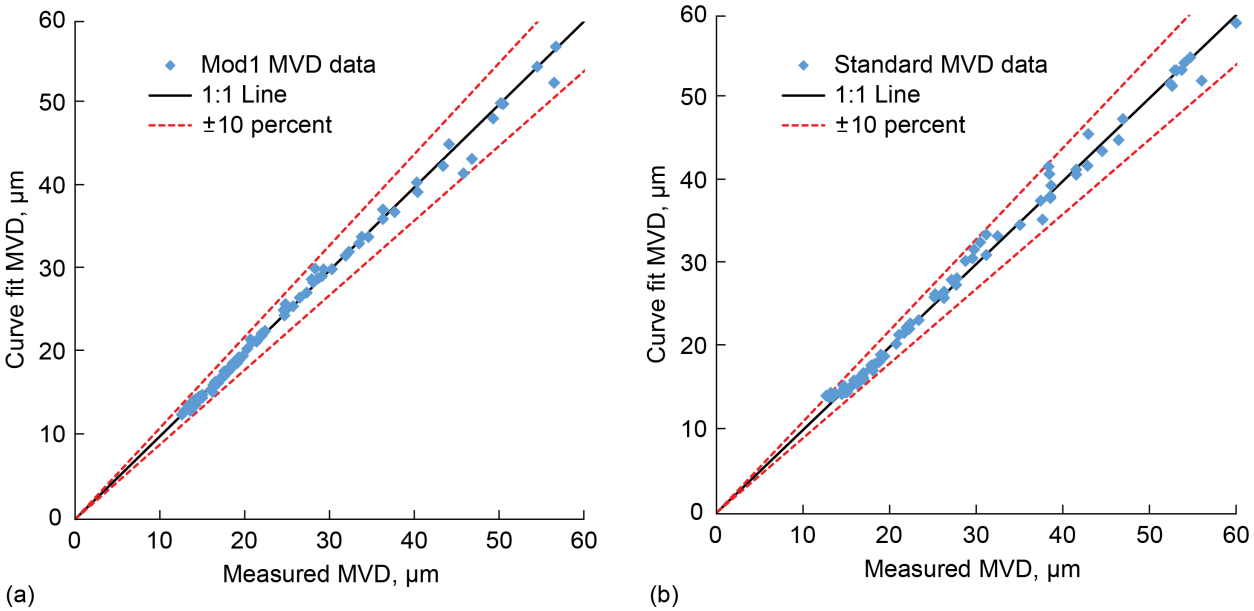

Figure 8.—Curve fit values from generated equations compared to measured values for Federal Aviation Administration (FAA) 14 CFR Parts 25 and 29, Appendix C conditions. (a) Mod1 nozzles. (b) Standard nozzles. Median volumetric diameter (MVD).

4.3 Supercooled Large Drops in Icing Research Tunnel

A third equation was generated for larger drops (Appendix O). Large drops are achievable by reducing the spray nozzle atomizing air pressure so there is less breakup of the water stream. Operating the Mod1 nozzles between $2 \le P_{air} \le 8$ psig is referred to as "SLD conditions" in the IRT referring to the definition of terms specified in Federal Aviation Administration (FAA) AC 25-28 (Ref. 6).

The drop-size distributions for SLD conditions were measured by combining data from the CDP, OAP–230X, and OAP–230Y. The SLD curve fit equation is

$$\begin{aligned} \mathrm{MVD_{SLD}} = a + bP_{\mathrm{air}} + c\ln(\Delta P) + dP_{\mathrm{air}}{}^2 + e\left[\ln(\Delta P)\right]^2 + fP_{\mathrm{air}}\ln(\Delta P) \\ + gP_{\mathrm{air}}^3 + h\left[\ln(\Delta P)\right]^3 + iP_{\mathrm{air}}\left[\ln(\Delta P)\right]^2 + jP_{\mathrm{air}}^2\left[\ln(\Delta P)\right] \end{aligned} \tag{3}$$

where a = 146.143887, b = –90.07027, c = 68.6842069, d = 16.8400043, e = –23.555536, f = –7.0109318, g = –1.1765187, h = 11.5895479, i = –6.4025056, and j = 2.33378761.

Figure 9 summarizes the MVD curve fits for the SLD operating range. Figure 9(a) shows the curve fit lines as a function of ΔP for each P_{air} line. Measured MVDs are also plotted against their respective curve fits for three P_{air} lines. Figure 9(b) shows the MVD goodness of fit, plotting how the curve fit values compare to the measured MVD. For Appendix O criteria, the IRT was able to fit the data to a curve within ±20 percent, shown in the figure as well. Comparisons of the IRT distributions to the FAA Appendix O (Ref. 4) requirements are shown in Figure 10 for both Freezing Drizzle (FZDZ) and Freezing Rain (FZRA) conditions.

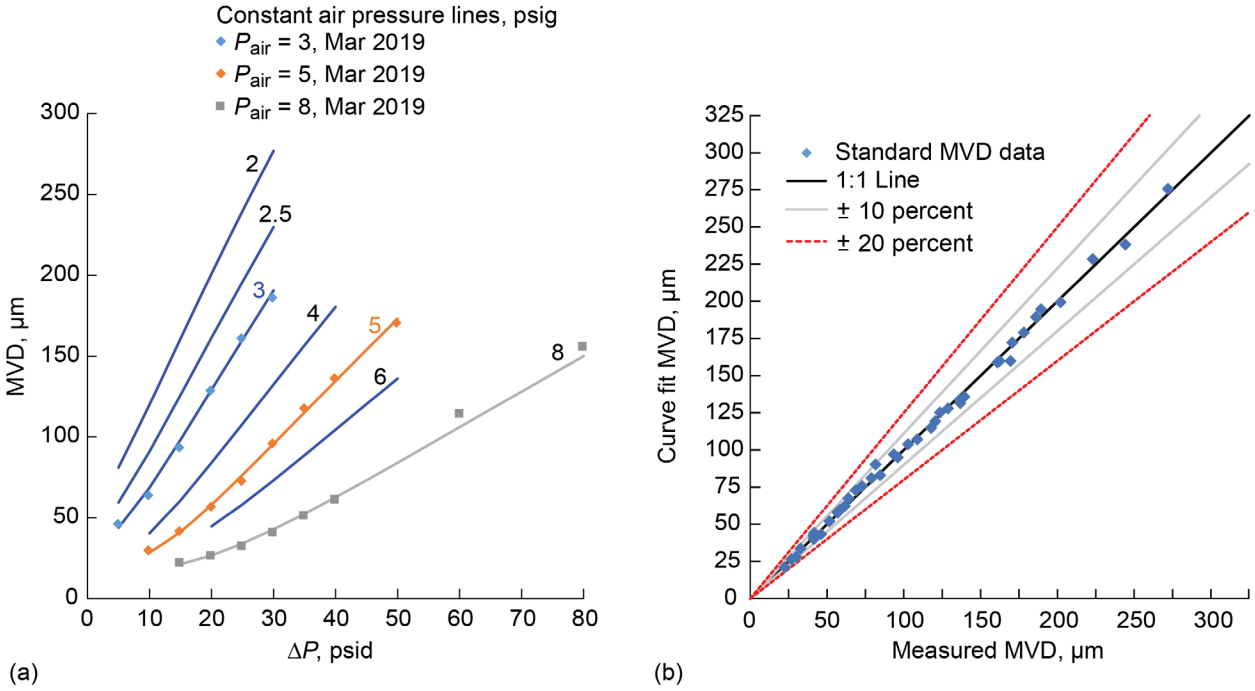

Figure 9.—Curve fit values from the generated equations compared to the measure values for Federal Aviation Administration (FAA) 14 CFR Parts 25 and 29, Appendix O conditions. (a) Median volumetric diameter (MVD) curve fits for supercooled large drop (SLD) as a function of ΔP for each atomizing air pressure (P_{air}). (b) Measured values for SLD conditions.

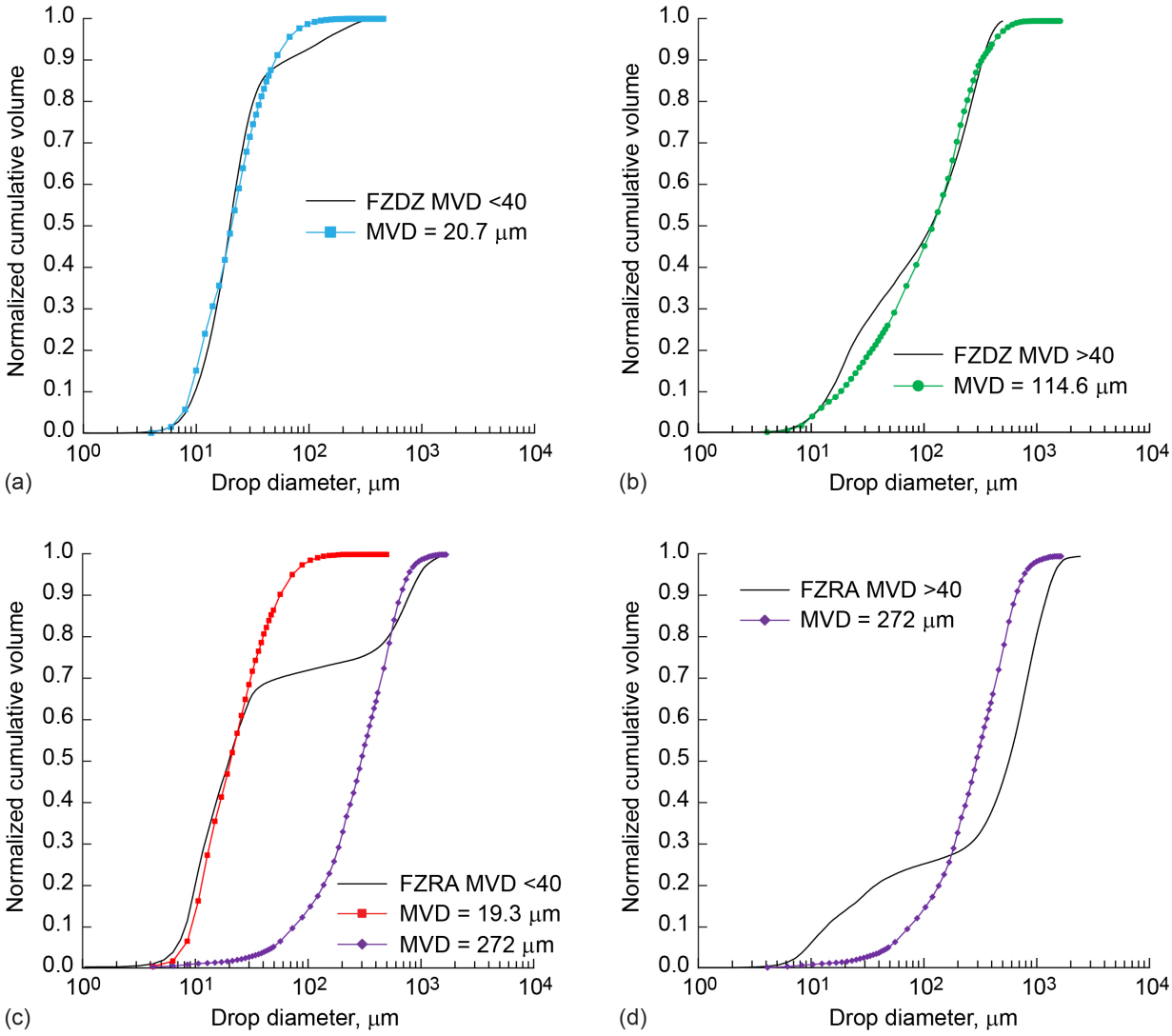

Figure 10.—Icing Research Tunnel (IRT) distributions to Federal Aviation Administration (FAA) 14 CFR Parts 25 and 29, Appendix O requirements for both Freezing Drizzle (FZDZ) and Freezing Rain (FZRA) conditions. (a) FZDZ, median volumetric diameter (MVD) <40 μm. (b) FZDZ, MVD >40 μm. (c) FZRA, MVD <40 μm. (d) FZRA, MVD >40 μm.

The IRT has also created a bimodal distribution similar to the FAA Part 25, Appendix O, FZDZ, MVD <40 μm condition. In Reference 7, it was found that when the IRT Mod1 and Standard nozzles are sprayed simultaneously, the combined spray distribution is a close match to the mathematical summation of the individual drop-size distributions. That is, there was no distinguishable effect of drop breakup or coalescence from spraying the two nozzle sets simultaneously. This information has been utilized to create additional variations of bimodal distributions by simultaneously spraying other Mod1 and Standard nozzle conditions as well. Further explorations have been done by Potapczuk and Tsao (Refs. 8 to 11). Recall that the IRT has one air manifold and two water manifolds in each spray bar, which means simultaneous-spray conditions require using the same nozzle air pressure for both Mod1 and Standard nozzles. Simultaneous sprays are likely to result in high LWC values, meaning scaling work will be required for tests that seek to match the FZDZ, MVD <40 μm conditions. During the 2019 full calibration, additional simultaneous spray conditions were identified that approximate the Appendix O FZDZ, MVD <40 μm, shown in Figure 11. Figure 11(a) shows four distributions to demonstrate that the simultaneous spray (Cond 24 Mod1 + Std) matches the mathematical summation of the constituent sprays, Mod1 (Cond 21 Mod1) and Standard (Cond 18 Std). Here, these two distributions match within 1.1 percent at all drop diameters. Figure 11(b) shows a simultaneous-spray condition measured in 2019 intended to match the FAA Appendix O, FZDZ, MVD <40 μm condition. In Figure 11(b), the mathematical summation matches the combined-spray distribution within 4 percent for all diameters, and the combined-spray distribution matches to FZDZ, MVD <40 μm within 9 percent for all drop diameters. The cloud uniformity and LWC values for bimodal conditions were also described in Reference 7. Cloud uniformity resembles other Standard-nozzle clouds, like that shown in Figure 3. Similar to drop-size distributions, the LWC values from the measured simultaneous sprays have been found to match the summation of the constituent sprays. The LWC for Cond 10 in Figure 11(b) is 1.31 g/m^3 at 250 kn.

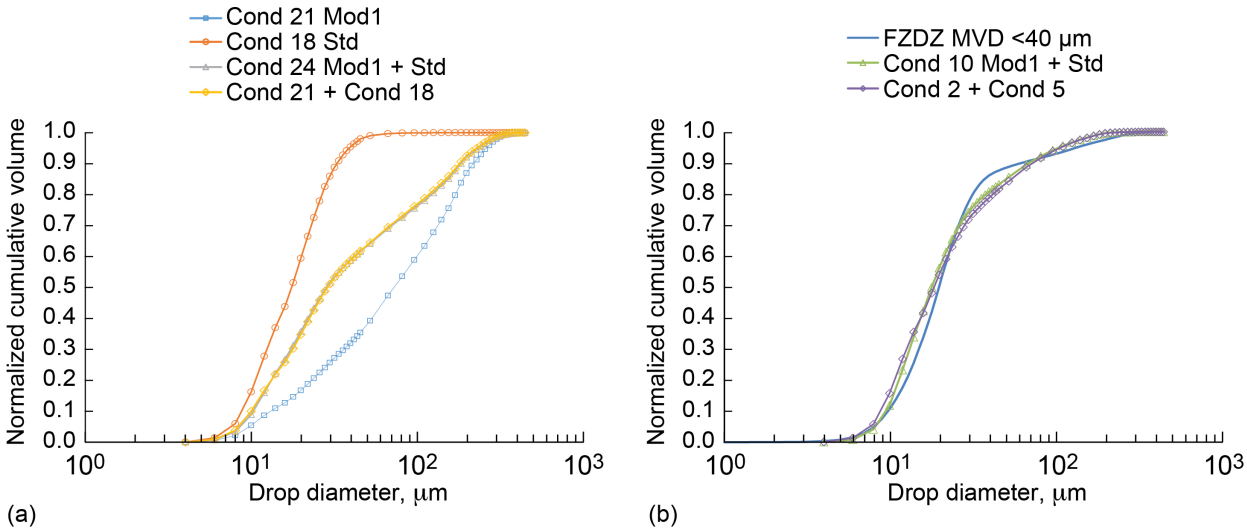

Figure 11.—Bimodal distributions that can be created in Icing Research Tunnel (IRT) by simultaneously spraying Mod1 and Standard (Std) nozzles with same nozzle air pressure. Mathematical summations of individual contributing sprays are shown alongside measured distributions from simultaneous sprays. (a) IRT's strongest bimodal case; includes two individual sprays and their simultaneous-spray results. (b) IRT 2019 distribution matching to Freezing Drizzle (FZDZ), median volumetric diameter (MVD) <40 μm.

5.0 Liquid Water Content Calibration

The Multi-Element Sensor (commonly known as the multi-wire) manufactured by Science Engineering Associates, Inc. (SEA, Inc.), was used to measure cloud LWC. Pictures of this instrument are shown in Figure 12. The sensing elements are positioned inside a heated shroud that is approximately 1 in. (25.4 mm) in diameter. A typical multi-element shroud contains three sensing elements of various sizes, as well as a compensation wire. The elements, shown in greatest detail in Figure 12(b), are a 0.083-in.- (2.1-mm-) diameter hollow cylinder, 0.083-in.- (2.1-mm-) diameter forward-facing half-pipe (total water content or TWC) element, and a 0.021-in.- (0.5-mm-) diameter wire. A compensation wire is located behind the central element, parallel to the shroud. The compensation wire is designed to compensate for changes in atmospheric conditions, for example, temperature and pressure. It is intended to stay dry. Newer multi-element sensors employ a 0.083-in.- (2.1-mm-) diameter rear-facing half-pipe element in place of the hollow cylinder element. Greater details on the theory of operation of the instrument can be found in References 12 and 13.

Though the multi-wire has been used as the primary instrument to calibrate the IRT LWC since 2011, the 2019 multi-wire data was validated against measurements from an icing blade (hereon referred to as "the blade") that had previously been used to calibrate LWC in the IRT until 2011. The blade is an accretion-based instrument with dimensions of 0.125 in. (3.18 mm) wide by 6.06 in. (154-mm) long by 0.75 in. (19.05 mm) thick. It is mounted in such a way that it is located at the horizontal centerline and the vertical center of the test section. It is run at a tunnel total air temperature between –0.4 and –4 °F (–18 and –20 °C) in an attempt to ensure that rime ice is accreted on the 0.125-in. (3.18-mm) flat face in most cases. Prior to use of the multi-wire as the primary instrument, the blade was the main LWC instrument of the IRT before 2011. It is described in detail in References 1 and 13.

Based on the results from Reference 13, further testing was done in 2016 to compare different mounts for the multi-wire. Particular focus was given to the measured water content values for the different conditions and configurations and how well they compared with blade measurements for low-impingement conditions (i.e., below the Ludlam limit for the blade). Tests were completed for both the

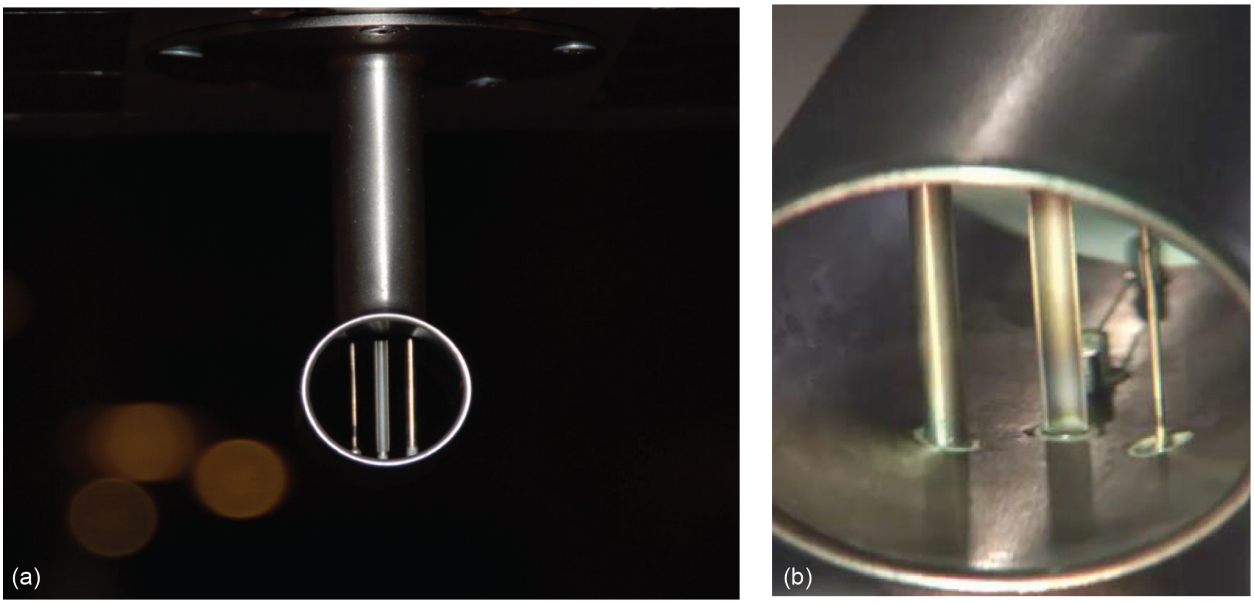

Figure 12.—Science Engineering Associates, Inc., Multi-Element Sensor. (a) Closeup view. (b) View of elements rotated 180° from (a).

Mod1 and Standard nozzle sets across the IRT's full range of airspeeds, MVDs, and nozzle air pressures. A more detailed discussion of these tests, as well as some of the added considerations, has been provided in the Appendix.

Ultimately, the test results showed that the multi-wire LWC measurements under a splitter plate were very comparable to measurements without a splitter plate when both were compared against the blade measurements at low water impingement rates. No conclusions could be drawn regarding which configuration gave more accurate measurements. Meanwhile, it was also noted that in high-impingement rates, it was difficult to keep the beveled leading edge of the splitter plate free from ice buildup, which results in artificial increase in the multi-wire measured LWC values. The rounded mast mount (i.e., without splitter plate; Figure 13) is easier to keep free of ice, which allows better ability to measure high-impingement conditions. This investigation was completed before the 2019 full calibration effort, leading to the decision to switch to the mast mount (without splitter plate). Even so, to confirm the accuracy of LWC measurements in this configuration, several data points were taken in 2019 with the icing blade for conditions below the blade's Ludlam limit, and these were compared to measurements with the multi-wire. Results are shown in Figure 14. Test conditions included velocities from 50 to 300 kn, MVD values from 15 to 50 μm, and nozzle air pressure values from 10 to 60 psig, all expected to be below the blade's Ludlam limit. The multi-wire data in this plot has been corrected for collision efficiency, as will be described in the following information.

Figure 13.—Multi-Element Sensor (Science Engineering Associates, Inc.) mount without a splitter plate.

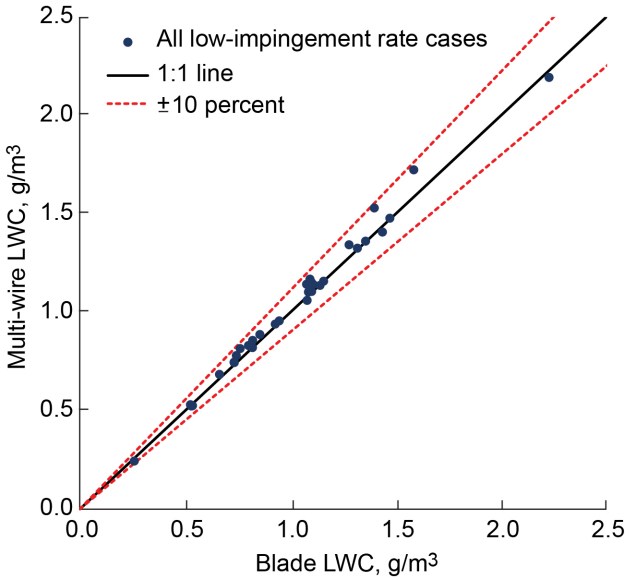

Figure 14.—Multi-wire data compared to icing blade data for low-impingement conditions (below icing blade's Ludlam limit) for 2019 multi-wire mounting configuration.

The IRT uses SEA Inc.'s M300 Data Acquisition System along with their WCM–2000 system to collect data from the multi-element sensor. The M300 records the power output of each of the sensing elements and receives the facility conditions from the facility control system, including total temperature, static temperature, airspeed, static air pressure, spray bar nozzle pressures, and whether the spray is on or off. All necessary calibration values and sensing element dimensions are received from the probe, and these are used along with the received facility conditions such that the data system can correlate the power of each sensing element to a calculated LWC. All the recorded values are output as 1 s averages into a CSV file. Once the data has been retrieved from the M300, it is postprocessed using a MATLAB® (The MathWorks, Inc.) code that was developed in-house. This code averages the data system outputs for each spray, starting 20 s after the spray begins and ending 2 s before the spray ends. A plot is generated for each spray so that the user may view the profile of the data and decide if the data seem reasonable. Further details can be found in Reference 13.

The smallest drops in the cloud are diverted around the sensing elements rather than impinging, particularly at low speeds, and so the measured LWC must also be corrected for the sensor's collision efficiency (also frequently called the collection efficiency). The primary sensor element used for LWC measurements in the IRT is the 2.1-mm-diameter forward-facing half pipe. In 2014, Rigby, Struk, and Bidwell (Ref. 14) modeled this sensing element along with the other two inside the multi-element sensor shroud using LEWICE3D, a particle trajectory code coupled with a three-dimensional (3D) flow-field analysis. They determined the correlation between the drop collision efficiency and the modified inertia parameter for drop diameters of 5, 20, 50, and 100 μm (Ref. 14). Struk then used this correlation to find total collision efficiency values based on particle size distributions measured in the IRT, rather than monodisperse drops (Ref. 15, personal communication). These values were in turn used to develop a formula for the collision efficiency correction as a function of MVD and airspeed in the IRT. Using this equation, collision efficiency corrections are applied to all data from the multi-element sensor to determine the actual cloud LWC based on the measured values. All the data in this report have been corrected with the collision efficiency correction based on the 3D geometry and the particle size distribution that was just described. This correction is only 1 to 2 percent for drop sizes larger than

100 μm at airspeeds above 100 kn, but the correction increases as drop size and airspeed decrease. The water content may be as much as 10 percent higher than measured for a drop-size distribution with an MVD of 20 μm at 100 kn. For a drop-size distribution with an MVD of 15 μm at 50 kn, the correction is greater than 15 percent.

The data from the TWC or half-pipe element of the multi-wire were corrected for collision efficiency according to the test point's particle size distribution and then compiled to build the LWC curve fits, correlating LWC to P_{air}, ΔP, and V. As described in the 2006 IRT calibration report (Ref. 5), the LWC calibration is a function of the form:

$$\mathrm{LWC} = K\left(V, P_{\mathrm{air}}\right)\frac{\sqrt{\Delta P}}{V} \tag{4}$$

where the surface function K is a function of V and P_{air}. Fitting the LWC curve involves determining the function K for both parameters, Ka and Kv. To define Kv, measurements were made from V = 50 to 300 kn while P_{air} and ΔP (and MVD) are held constant. Similarly, to determine Ka, V and MVD were held constant while making measurements from P_{air} = 10 to 60 psig. K is calculated for each of the measured values by rearranging Equation (4): $K = \mathrm{LWC}\left(V/\sqrt{\Delta P}\right)$. Once relationships are found, they are combined to determine the surface function, K, which is unique for the Mod1 and Standard nozzle sets, as well as the SLD conditions. In previous years, this relationship was linear but in 2019, a polynomial relationship was found. Equations (5), (6), and (7) are the respective equations for each.

$$\mathrm{LWC}_{\mathrm{Mod1}} = \left(a + bV^2 + cV + dP_{\mathrm{air}}{}^2 + eP_{\mathrm{air}}\right)\frac{\sqrt{\Delta P - i}}{V}\left(\frac{\mathrm{MVD} - f}{g}\right)^h \tag{5}$$

where a = 10.8, b = –0.00005, c = 0.0675, d = 0.0012, e = –0.17, f = 2, g = 24, h = 0.11, and i = 0.3.

$$\mathrm{LWC}_{\mathrm{Standards}} = \left(a + bV^2 + cV + dP_{\mathrm{air}}\right)\frac{\sqrt{\Delta P}}{V}\left(\frac{\mathrm{MVD} - e}{f}\right)^g \tag{6}$$

where a = 40.5, b = –0.0004, c = 0.2456, d = –0.2799, e = 4, f = 22, and g = 0.1.

$$\mathrm{LWC}_{\mathrm{SLD}} = \left(a + bV^2 + cV + dP_{\mathrm{air}}\right)\frac{\sqrt{\Delta P - e}}{V}\left(\frac{\mathrm{MVD}}{f}\right)^g \tag{7}$$

where a = 14.581, b = –0.00026, c = 0.132, d = –0.6092, e = 0.5, f = 120, and g = 0.11.

Figure 15(a) and (b) show the goodness of fit of the LWC equations for the Mod1 and Standard nozzle sets, respectively. These reference lines show that the curve fits agree with the majority of the data within ±10 percent, which is the target accuracy of the IRT. The SLD conditions have a target accuracy of ±20 percent but as seen in Figure 15(c), the LWC curve fit agrees with majority of the data within ±10 percent for SLD conditions.

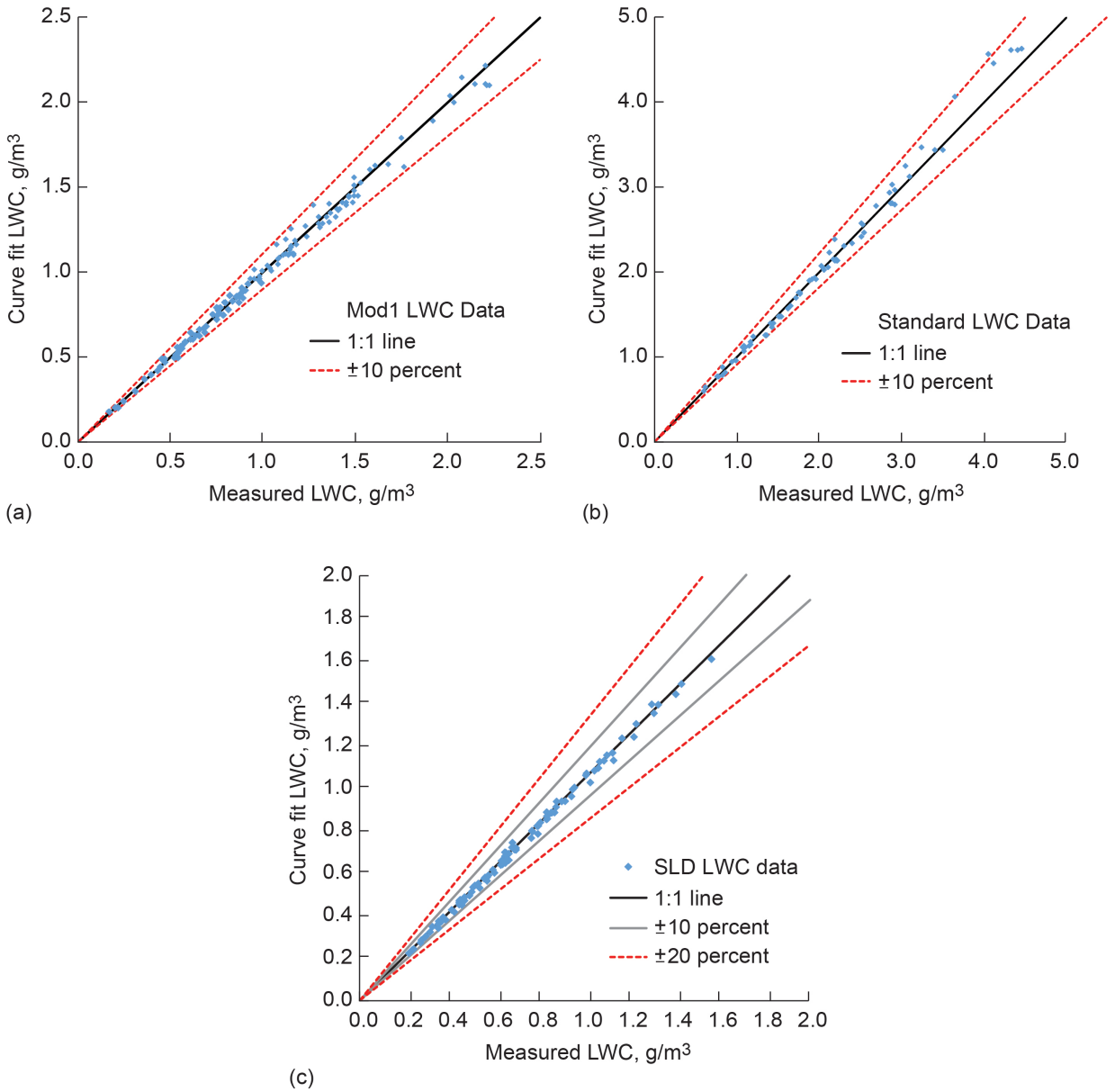

Figure 15.—Curve fit values from generated equations compared to measured values. (a) Mod1 nozzle set. (b) Standard nozzle set. (c) Supercooled liquid drop conditions (SLD). Liquid water content (LWC).

6.0 Findings From Subsequent Check Calibrations

The IRT has completed two check calibrations following the full calibration based on recommendations from SAE ARP5905 (Ref. 1). The first was in January 2020, the second in March 2020, and each included grid and multi-wire measurements to check cloud uniformity and LWC, respectively. Test matrices included a small subset of full-calibration test conditions that could be checked utilizing 1 test day per instrument.

Overall, the vast majority of results from the check calibrations showed the cloud uniformity and LWC were repeating well to the full-calibration measurements. Cloud uniformity measurements for baseline conditions repeated within ±10 percent of values taken during the full calibration. In measuring LWC with the multi-wire, 52 out of 55 test conditions were consistent with expectations and measured

within ±10 percent of the values measured during the full calibration. In actuality, 44 out of 55 test conditions repeated very well, within ±3 percent of the full-calibration values.

It must be reported, however, that a small section of the operating envelopes was found to be outside the stated calibration limits. This has been linked to conditions with $P_{air} \geq 10$ psig and $\Delta P \leq 10$ psid. The multi-wire LWC values for these conditions were measured in January and March 2020 and found to be 7 to 16 percent lower than previously measured, where anything more than 10 percent low is outside of the stated repeatability expectation of ±10 percent. A few Standard-nozzle uniformity conditions fitting these criteria were measured with the grid and confirmed these lower LWC values. The cause for this change is still under investigation, but the IRT expects to address the problem and take additional data as soon as possible. The calibration curves will be amended as necessary.

For tests that were conducted between September 2019 and March 2020 as long as test conditions do not match the pressure setting criteria described in the previous paragraph, the IRT staff still expects accuracy values of ±10 percent for LWC and MVD. Accuracy values for Mod1 nozzles with $P_{air} \leq 8$ psig (SLD conditions) are still expected to be ±20 percent.

7.0 Icing Cloud Operating Envelopes

The IRT's icing envelopes for both the Mod1 and Standard nozzles are compared to the FAA Appendix C icing criteria (Ref. 3) in Figure 16 for an airspeed of 225 kn. The operating envelopes for SLD conditions ($P_{air} \leq 8$ psig) are shown in Figure 17. Cloud LWC is airspeed dependent; at higher airspeeds, lower LWC values can be reached, and conversely so for lower airspeeds. This is demonstrated in Figure 17(a) and (b). The conditions specified in Figure 17(a) have also been plotted in Figure 16 to demonstrate how these nozzle settings may be used to reach lower LWC Appendix C conditions. It should be noted that SLD conditions are only calibrated for airspeeds between 100 to 250 kn, unlike Appendix C conditions, which are calibrated for airspeeds between 50 to 300 kn. Additionally, MVD and LWC uncertainty for SLD conditions is ±20 percent rather than ±10 percent for $P_{air} \geq 10$ psig. Cloud size also tends to be smaller, and uniformity might not be as good, depending on the test condition, as can be seen from comparing Figure 3(a) and (c).

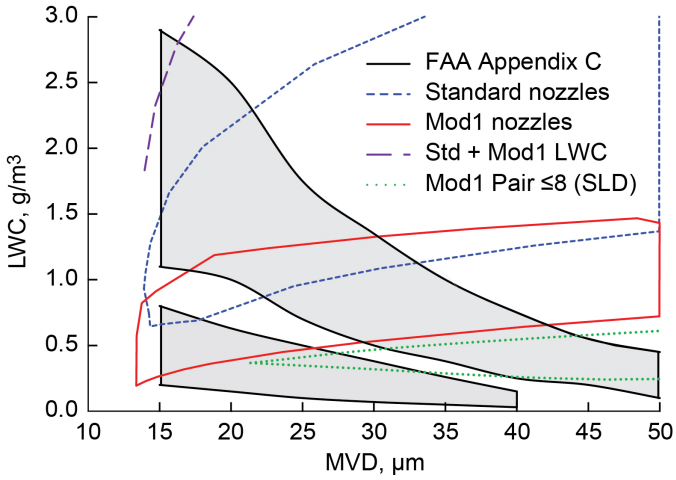

Figure 16.—2019 Icing Research Tunnel operating envelopes for airspeed of 225 kn with median volumetric diameter (MVD) <50 μm compared against Federal Aviation Administration (FAA) 14 CFR Parts 25 and 29, Appendix C envelopes. Liquid water content (LWC). Supercooled liquid drop (SLD). Standard (Std).

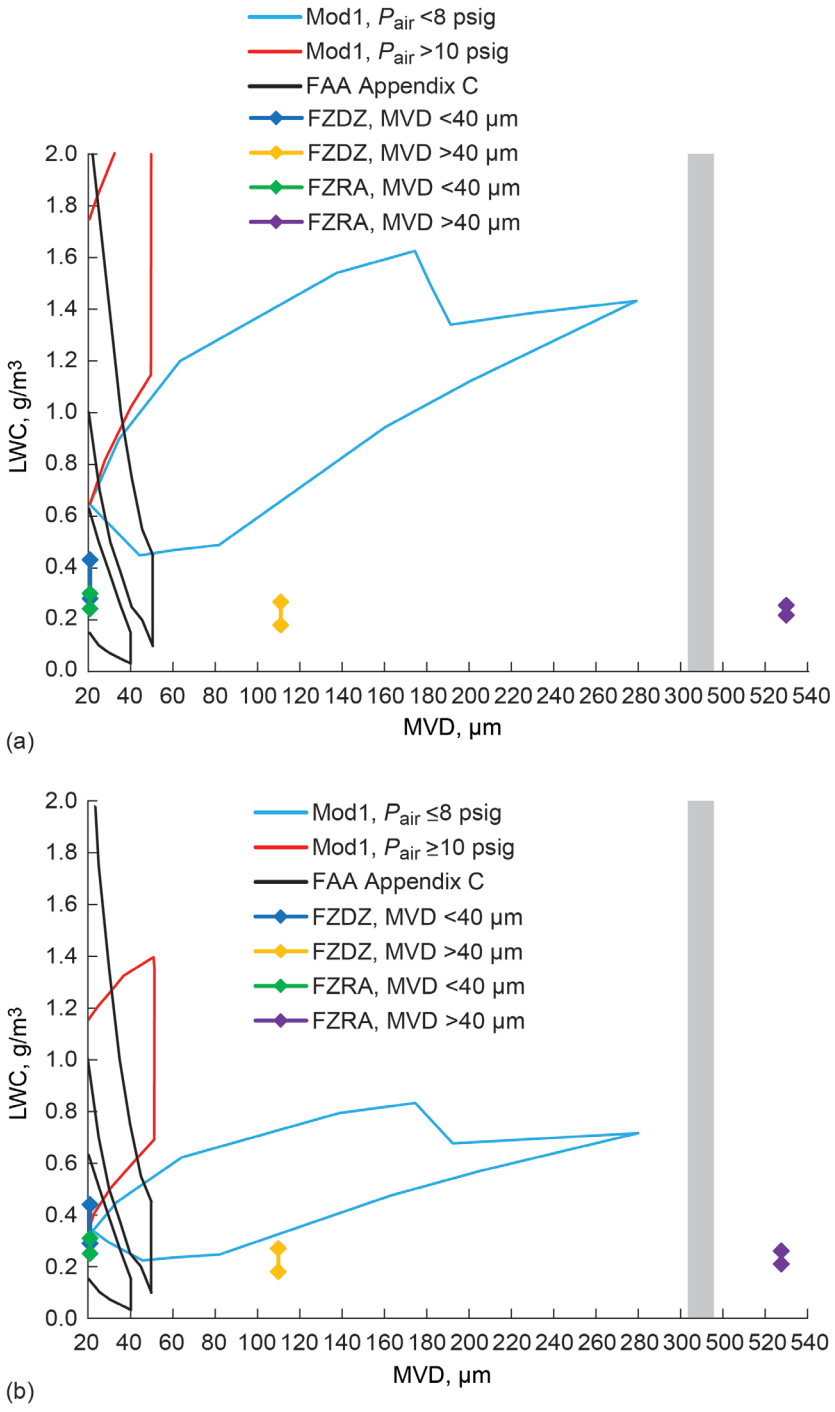

Figure 17.—2019 Icing Research Tunnel operating envelopes for different airspeeds compared to Federal Aviation Administration (FAA) 14 CFR Parts 25 and 29, Appendix C. For median volumetric diameter (MVD) 15 to 50 µm, see 14 CFR Parts 25 and 29, Appendix C operating envelope. (a) 100 kn. (b) 250 kn. Freezing Drizzle (FZDZ). Freezing Rain (FZRA). Liquid water content (LWC).

The operating envelopes for the SLD Appendix O conditions are shown in Figure 17(a) and (b), which also show the inversely proportional airspeed and LWC relationship. These two plots also indicate the FZDZ and FZRA conditions as specified by the FAA in Reference 4, according to their MVD values and LWC ranges. Those who wish to test FAA Appendix O conditions in the IRT may contact any of the authors of this report to discuss options.

8.0 Conclusion

The procedures and results of the full cloud calibration conducted in NASA Glenn's Icing Research Tunnel (IRT) from February to May 2019 have been described. The calibration came as a recommended practice from SAE's ARP5905 "Calibration and Acceptance of Icing Wind Tunnels" to perform a full calibration every 5 years. Uniform icing clouds were established with both the Mod1 and Standard nozzle sets and also supercooled liquid drop (SLD) conditions. The median volumetric diameter (MVD) and liquid water content (LWC) curve fits for both nozzle sets have been established and shown to be within the ±10-percent targets for Federal Aviation Administration (FAA) 14 CFR Parts 25 and 29, Appendix C conditions (nozzle air pressure ≥10 psig) and within the target accuracy of ±20 percent for SLD conditions (Mod1 nozzles with nozzle air pressure ≤8 psig).

A few changes were made to the IRT cloud calibration procedures, compared to those reported in 2015. The number of spraying Mod1 nozzles was increased from 88 to 103. The uppermost bins from the Cloud Droplet Probe (CDP; Droplet Measurement Technologies) and Optical Array Probe (OAP–230X; Particle Measuring Systems) were not used when there was larger scale probe data available. That is, the CDP was used for drop diameters up to 46 μm and the OAP–230X was used for drop diameters between 46 to 367 μm. The full calibration now includes testing a bimodal condition created by simultaneously spraying the Mod1 and Standard nozzles, which has been found to match the Appendix O Freezing Drizzle (FZDZ), MVD <40 μm condition within 9 percent. Finally, the splitter plate was removed from the multi-wire test configuration because it was found to have indiscernible improvement to the data accuracy and also caused contamination of high-impingement case measurements when there was substantial ice buildup on the leading edge. Further discussion of the reasoning behind this change is in the included Appendix.

Appendix—Considerations and Decision Points Regarding Splitter Plate for Multi-Wire Mount

The Multi-Element Sensor (commonly known as the multi-wire; Science Engineering Associates, Inc. (SEA, Inc.)) has been the primary instrument for the Icing Research Tunnel's (IRT's) liquid water content (LWC) calibrations since 2011, as described in Reference 13. Reference 13 included an in-depth discussion of the original IRT data that instigated the addition of a splitter plate to the multi-wire mounting strut. However, the LWC data leading to that decision were not highly conclusive. The following Appendix may be considered an extension of the splitter plate data presented in Reference 13 or as a standalone discussion of more recent tests that were conducted to compare multi-wire measurements under different mounting configurations to LWC measured by the icing blade (referred to as "the blade"). The primary goal of these tests was to assess data accuracy compared to the blade using the more appropriate multi-wire collection efficiency corrections that were established in 2014, as done retroactively in Reference 13 (published in 2016 to discuss 2009 data). Test conditions included the full range of IRT airspeeds (50 to 300 kn), spray nozzle air pressures (2 to 60 psig), and drop sizes (median volumetric diameter (MVD) values between 15 and 270 μm). Data accuracy tests were largely inconclusive, particularly since variations in the data were often lower than the repeatability that was observed. It was also found that the beveled splitter plate was most difficult to keep free of ice in high-impingement scenarios. This led to data biasing if the ice buildup reached the underside of the leading edge in front of the sensor. Other considerations included computational flow-field studies and the possibility of element shadowing, neither of which indicated one configuration as more accurate than another. Ultimately, the IRT staff decided to use the multi-wire without a splitter plate for the 2019 full calibration because there was no discernible difference in the data accuracy, and the leading edge of the beveled splitter plate was more difficult to keep free of ice. It may also be noted that there were multiple instances of ice shedding into the multi-wire shroud while testing without the splitter plate, but none of these were found to be damaging to the instrument.

Test Setup

The three different multi-wire mounting configurations that were tested are shown in Figure 18. The first was under a 0.25-in.-thick splitter plate with a beveled leading edge (the same configuration used for calibration testing since 2011) with a Minco heater adhered to the top surface of the leading edge (edges secured with aluminum foil tape). The second splitter plate configuration was under a 0.375-in.-thick splitter plate with a rounded, half-cylinder leading edge (radius of curvature: 3/16 in.) and was slightly thicker than the first in order to accommodate five, 0.25-in.-thick cartridge heaters installed across the span. The rounded leading edge was chosen because it is easier to maintain temperature for a rounded leading edge than a sharp one, and because a rounded leading edge would be less prone to flow separation with downward flow angularity. The third configuration was the multi-wire without a splitter plate, mounted directly under the strut. Each configuration utilized the same strut that had a 5- by 3.5-in. elliptical cross section, large enough to house the multi-wire connection box. The length of the strut was consistent so that the center of the multi-wire elements would be positioned at test section center. Minco heaters were adhered onto the strut to prevent and deter ice accretion.

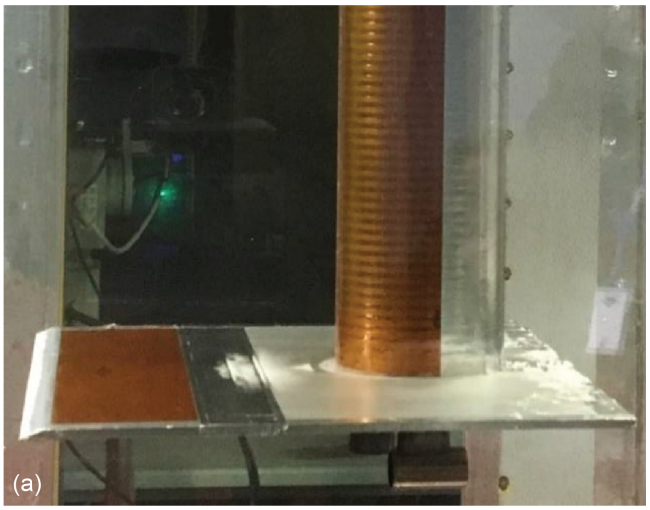

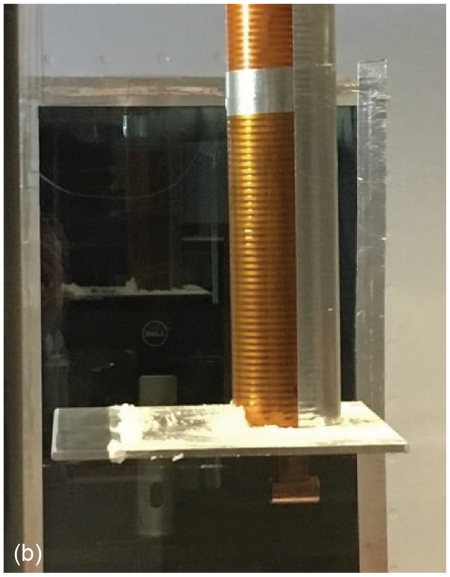

Figure 18.—Multi-wire mounting configurations tested in 2016. (a) Beveled leading edge (used in Icing Research Tunnel from 2009 to 2018). (b) Rounded leading edge. (c) No splitter plate.

The primary goal of these tests was to determine which of these configurations led to the most accurate data, that is, which configuration yielded results that compared the best with the blade when conditions were below the blade's Ludlam limit. Tests were conducted for both IRT nozzle types (Standard and Mod1) for an airspeed range of 50 to 300 kn, and for the full range of nozzle air pressures. Further testing included high-impingement-rate conditions (spraying both nozzle sets simultaneously) and larger MVD values. The blade cannot give accurate LWC measurements under the two latter conditions, but there was still a desire to compare multi-wire measurements for the different configurations. Secondary considerations included propensity for ice buildup on the leading edge, flow-field calculations, additional contamination of multi-wire data due to shadowing or splashing, steadiness of the readings, and ice shedding into the multi-wire shroud.

Data Processing and Canonical Values

The data in this Appendix were processed in the same way as stated in the main text of this report. For the multi-wire, all LWC values that were used were measured by the total water content (TWC) element, that is, the forward-facing half-pipe element with a 2.1-mm diameter. LWC values were received through the M300 system (SEA, Inc.) and averaged starting 20 s after the spray turned on through 2 s before the spray turned off. Measured values were tared by subtracting the 10-s average of the prespray values. Averaged TWC values were corrected for collision efficiency using the values computed in 2014 by Rigby, Struk, and Bidwell from three-dimensional particle trajectory analyses as well as IRT particle size distributions (Refs. 14 and 15). For the blade, three measurements were made of the accretion thickness, and the median thickness value was used along with airspeed and spray duration to calculate LWC. Blade LWC values were corrected for collection efficiency calculated by the FWG Associate, Inc., two-dimensional particle trajectory code (Ref. 16). Further details on data processing can be found in Reference 13.

Additionally, a canonical correlation analysis was used for the blade and multi-wire LWC data in this Appendix. When facility setpoints do not exactly equal the target (as is usually the case), there is transmission of error (Refs. 17 and 18), for example, an airspeed of 149.4 kn instead of 150.0 kn will cause a slight increase to the measured LWC. For more adequate comparison between like conditions, the data have been made canonical by quantifying the expected transmitted error and removing it from the value that is measured by the instrument. Corrections were made assuming a linear correlation in differences when the setpoints are close, and were made using the format

$$c_{\text{measured}} - c_{\text{canonical}} = f_{\text{measured}} - f_{\text{canonical}}$$

where c represents the LWC value calculated from the IRT calibration equations using true airspeed velocity (V), spray nozzle atomizing air pressure (P_{air}), and spray nozzle water pressure minus P_{air} (ΔP) and f represents measured values from the instrument; canonical corresponds to target setpoint values and measured corresponds to the actual facility conditions that were created. That is, the target setpoint values were used to calculate $c_{\text{canonical}}$ and the actual facility values measured during the test were used to calculate c_{measured}. The value f_{measured} represents the LWC value measured by the multi-wire, which corresponds to the measured facility condition values. The value $f_{\text{canonical}}$ represents the canonical value, with the intention that $f_{\text{canonical}}$ would have been the measured value if the setpoints had been met exactly. The resulting $f_{\text{canonical}}$ values are what are compared in this Appendix. Making this correction allows better comparison of like conditions even though facility setpoints are generally not equal to the targeted test conditions. Out of the 215 conditions that were made canonical, 83.7 percent changed by less than 1 percent, 12.6 percent changed by 1 to 2 percent, 3.3 percent changed by 2 to 3 percent, and less than 1 percent changed by more than 4 percent. All of the LWC data discussed in this Appendix are $f_{\text{canonical}}$ values, with the exception of the data traces shown in the sections “Effect of Ice Buildup on Leading Edge” and “Possibility of Ice Shedding”.

Repeatability of Icing Research Tunnel and Liquid Water Content Instrumentation

Given the amount of scatter that was observed within the test data, it is critical to consider the expected repeatability of the instrumentation and the IRT cloud. Two test conditions (one with Mod1 and one with Standard nozzles) were repeated four times with the three multi-wire configurations as well as the blade (with one exception: only three successful repeats were collected with the blade for the Standard nozzle condition). While this number of data points does not constitute a statistically significant sampling,

it may give a starting idea for repeatability. Figure 19 shows a comparison of repeat data from the Mod1 and Standard nozzles, while Table I shows the tabulated results along with the computed average and the range normalized by the average. The average range that was recorded for each condition was 6 percent of the average recorded LWC value.

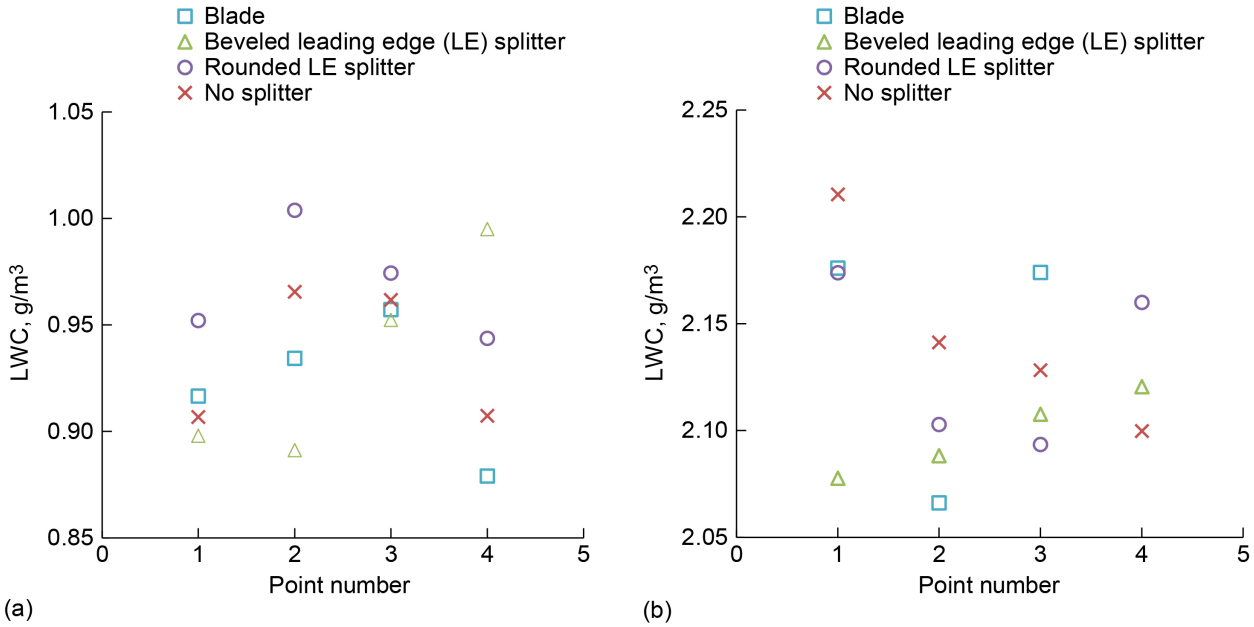

Figure 19.—Liquid water content (LWC) values measured by icing blade and multi-wire under three configurations for single Mod1 and Standard nozzle test condition repeated four times throughout day. Airspeed = 150 kn. Median volumetric diameter = 21 μm. Spray nozzle air pressure = 30 psig. (a) Mod1 nozzles. (b) Standard nozzles.

TABLE I.—TABULATED RESULTS FROM REPEAT POINTS FOR MOD1 AND STANDARD NOZZLES LIQUID WATER CONTENT (LWC)

[Airspeed = 150 kn. Median volumetric diameter = 21 μm.]

Point number	Mod1 nozzles LWC, g/m^3				Standard nozzles LWC, g/m^3			
	Blade	Beveled leading edge (LE)	Rounded LE	No splitter	Blade	Beveled LE	Rounded LE	No splitter
1	0.92	0.90	0.95	0.91	2.18	2.08	2.17	2.21
2	0.93	0.89	1.00	0.97	2.07	2.09	2.10	2.14
3	0.96	0.95	0.97	0.96	2.17	2.11	2.09	2.13
4	0.88	1.00	0.94	0.91	------	2.12	2.16	2.10
LWC average	0.92	0.93	0.97	0.94	2.13	2.09	2.14	2.16
(Maximum – minimum)/average	0.085	0.111	0.062	0.063	0.051	0.020	0.038	0.052

Measurements Compared to Icing Blade, Varying Airspeed, and Nozzle Air Pressure

Figure 20 and Figure 21 show LWC comparisons from the three configurations with respect to *V*. The MVD is approximately 21 μm for all cases, and P_{air} was constant at 30 psig. Figure 20 shows the ratio of multi-wire LWC values compared to the blade for Mod1 and Standard nozzles and omits data when there was indication the blade was undermeasuring, likely because the conditions are near or above the Ludlam limit. In Figure 20(a) showing the Mod1 nozzles for all three configurations, the measured multi-wire LWC values average slightly higher than the blade LWC. The range of ratios observed (beveled splitter: 0.092, rounded splitter: 0.032, and no splitter: 0.045) is less than the respective normalized range for the Mod1 repeat conditions in Table I, so data trends may not be significant. In Figure 20(b) for all three airspeeds, the measured multi-wire LWC values average lower than the blade LWC. The range of ratios observed (beveled splitter: 0.038, rounded splitter: 0.041, and no splitter: 0.066) are fairly comparable to their respective values in Table I, sometimes higher and sometimes lower. In these two plots, the LWC from both the no-splitter and rounded-splitter configurations remain within about ±5 percent of the blade LWC, while the beveled-splitter configuration remains within about ±7 percent of the blade LWC values. Figure 21 shows the same data as Figure 20 but also includes higher airspeed conditions. For these plots, the multi-wire LWC values have been normalized by the average LWC from all three multi-wire configurations for each test condition. This also means that for each condition, the three ratio values will average to be 1.0. As with Figure 20, it is difficult to discern consistent trends. Two things that may be noted are (1) in Figure 21(a) with Mod1 nozzles, all configurations are within ±4 percent of the average LWC for each condition and (2) in Figure 21(b), the rounded-splitter and no-splitter configurations are within ±3 percent; the beveled leading edge splitter performs differently from the other two for airspeeds of 150 kn and higher, but it is still within ±5 percent of the average.

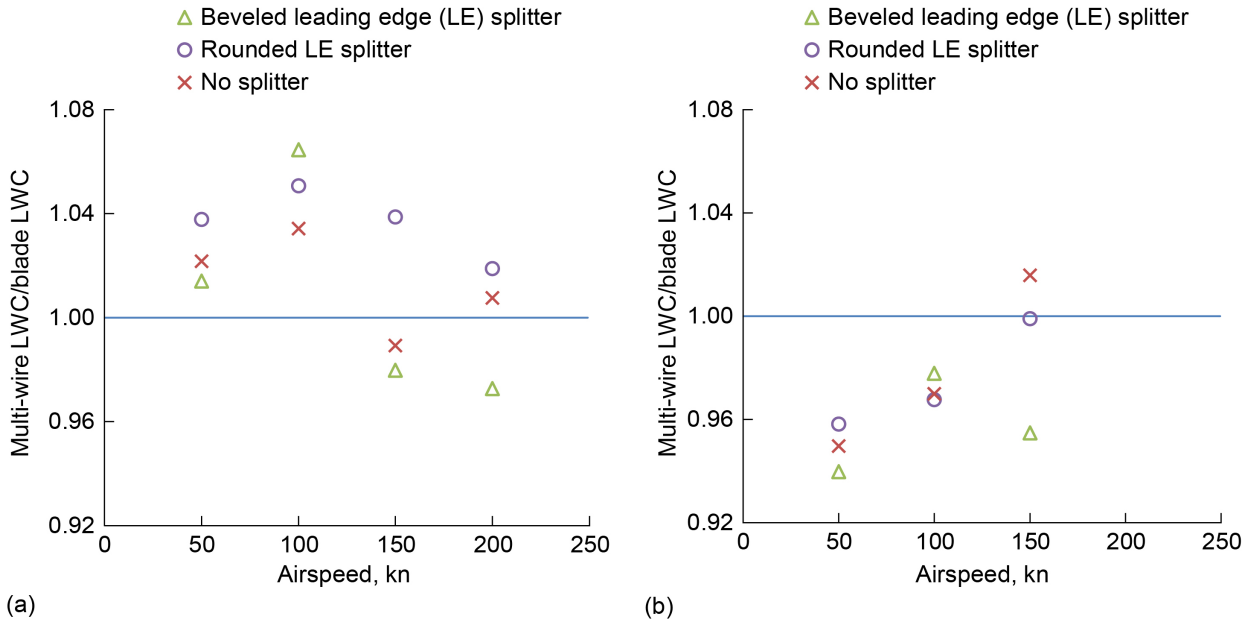

Figure 20.—Multi-wire liquid water content (LWC) data at range of airspeeds for all three mounting configurations, normalized by icing blade LWC values. Higher airspeed values were omitted as it was expected the blade was undermeasuring LWC. (a) Mod1 nozzles. (b) Standard nozzles.

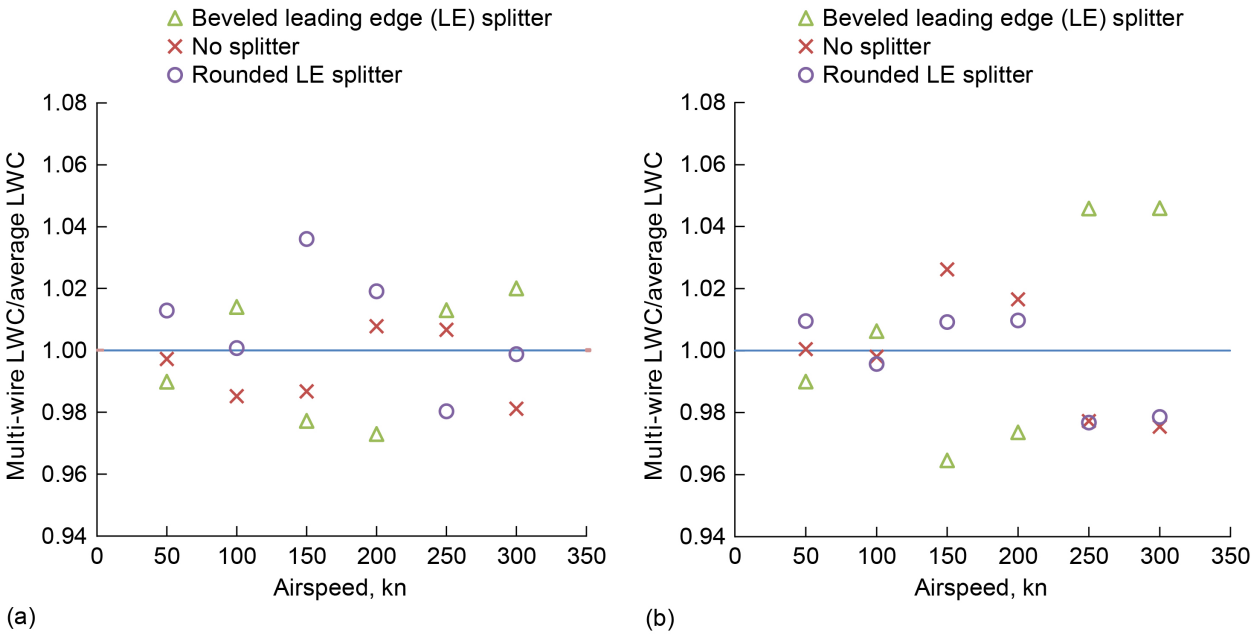

Figure 21.—Multi-wire liquid water content (LWC) data for full range of airspeeds for all three configurations, normalized by average LWC measured by multi-wire under three configurations for each condition. Plots contain all data shown in Figure 20, as well as higher airspeed conditions. (a) Mod1 nozzles. (b) Standard nozzles.

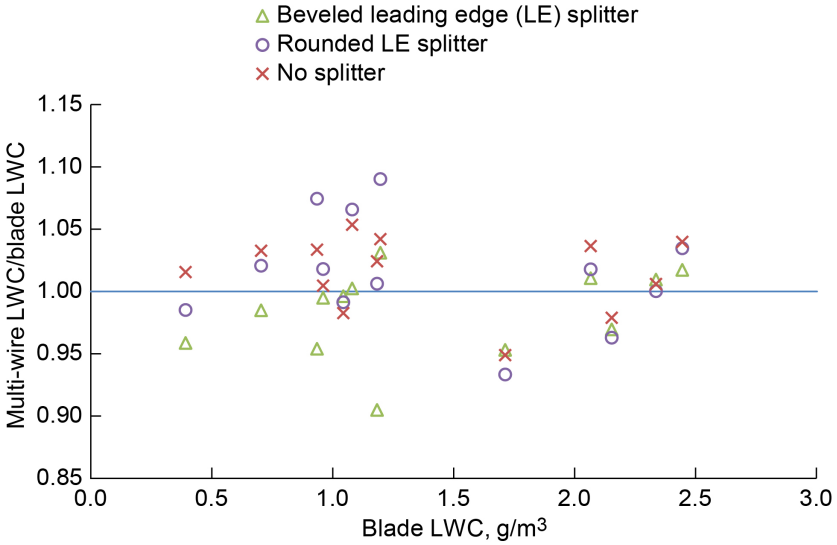

Figure 22.—Mod1 and Standard nozzle liquid water content (LWC) data at median volumetric diameter of approximately 20 μm and airspeed of 150 kn for spray nozzle air pressures 10 ≤ P_{air} ≤ 60 psig.

Figure 22 shows multi-wire LWC measurements normalized by the blade LWC for both nozzle sets at 150 kn with a MVD of approximately 20 μm. P_{air} values range from 10 to 60 psig. Similar to the previous plots, this plot is also not conclusive, but it may be noted that the LWC for the no-splitter configuration remains within ±6 percent of the blade LWC, while the LWCs for the beveled and rounded splitter configurations do not. For LWC values below 1.5 g/m^3, LWC measured with the beveled splitter plate tends to be lower than the other two configurations and also lower than the blade.

Overall, the levels of variation observed are comparable to the levels of variation seen from the repeat points in Table I, making it difficult to form conclusions about any configuration being more accurate than another.

Comparing Multi-Wire Liquid Water Content in Different Configurations, Varying Median Volumetric Diameter

Further testing was conducted by varying the MVD values at three different airspeeds. Reference 13 indicated the blade tends to undermeasure at MVD values higher than 50 μm, potentially as low as 30 μm. Hence, for these cases, the multi-wire was compared to itself, again normalizing by the average LWC from all three configurations, with the intent of looking for trends that might indicate performance. Results are shown in Figure 23. Here, the multi-wire under the beveled splitter plate measures LWC values an average of 3 percent higher than the average LWC from all three configurations. The other two configurations tended to be more consistent with each other. In the absence of trustworthy blade data, it is difficult to know which configuration was most accurate. Figure 23 could suggest that drop trajectories with the beveled splitter plate lead to higher impingement on the sensor head for most airspeeds and drop sizes. However, it is odd that these results seem inconsistent with those in Figure 22, particularly for LWC <1.25 g/m^3, most of which were created by the Mod1 nozzles (as the conditions in Figure 23 were) and which indicated the LWC values with the beveled splitter were lower than the LWC from the other two configurations. There was one Mod1 condition tested in all three configurations with a nozzle air pressure of 30 psig, an MVD of 21.7 μm, and an airspeed of 150 kn, for which the recorded values are shown in both Figure 22 and Figure 23. In Figure 23, the LWC for this condition with the beveled splitter plate is 7 percent lower than the average LWC. Since most other beveled splitter plate LWC values averaged at 3 percent high, this is 10 percent lower than other conditions for the same configuration, and it appears to be an outlier. But in Figure 22, this condition is represented twice (blade LWC approximately 0.95 g/m^3) and the LWC with the beveled leading edge is 5 and 1 percent lower than corresponding blade LWC, where the average ratio for the Mod1 conditions shown there is 2 percent lower than the blade for Mod1 conditions, that is, the values are fairly consistent with other values and do not suggest the condition is a strong outlier. Hence, the immediate implications from Figure 23 may not be as conclusive as they appear to be. While Figure 23 may suggest that drop trajectories with the beveled splitter plate lend to higher LWC for most airspeeds and drop sizes, the data also suggest that impingement is lower for a particular airspeed and drop size, that is 150 kn and MVD = 20 μm, studied in Figure 22, which is in the middle of typical IRT cloud conditions, and where several key cloud calibration test points are typically taken. To have an inconsistency here could be detrimental to cloud calibration accuracy. The rounded splitter plate LWC values appear to show the converse of this; LWC ratios in Figure 23 average to be lower than the blade, with an apparent outlier at 20 μm that is 5 percent higher than the blade, and Mod1 nozzle LWC ratios in Figure 22 averaging to be higher than the blade. Meanwhile, LWC ratios from the no-splitter configuration appear to be more consistent between the two figures, remaining within about ±5 percent in both Figure 22 and Figure 23.

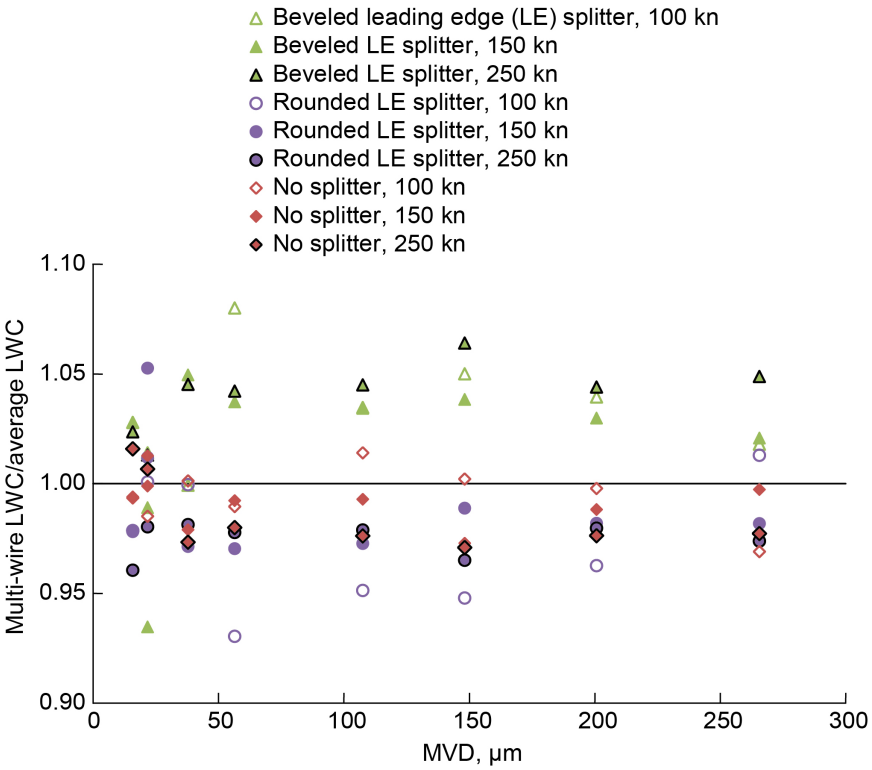

Figure 23.—Comparison of multi-wire data under three configurations for full range of median volumetric diameter (MVD) values at three airspeeds. All conditions are with Mod1 nozzles. Multi-wire data is normalized by average value from three configurations for each condition. Liquid water content (LWC). Leading edge (LE).

Effect of Ice Buildup on Leading Edge

While the primary goal for these tests was to address instrument accuracy compared to the blade, other considerations were investigated as well. This test also investigated the ability of each configuration's heaters to keep the leading edge free from ice buildup, and also look for any effects due to ice buildup on the leading edge. It was briefly noted in Reference 13 that if ice builds up on the leading edge of the splitter plate and extends below the leading edge in front of the sensor, like that seen in Figure 24, it causes the multi-wire to read artificially high LWC values. This can be recognized in the multi-wire data when the water content readings start increasing for all three vertical elements and there is no simultaneous decrease in compensation wire power. Figure 25 shows an example of this as observed with the 250-kn condition tested with the beveled splitter plate. Correspondingly, Figure 26 shows the multi-wire TWC element data for the same test condition measured under the three different multi-wire configurations. For this condition, the TWC values from the beveled leading edge show a gradual increase, such that by the end of the spray, the LWC is higher than that measured from the other two configurations. Figure 27 shows averaged results from six different high-impingement-rate conditions. The data in Figure 27 confirm the observations seen in Figure 25 and Figure 26: the beveled splitter plate tends to measure higher than the other two configurations, particularly for the 250-kn cases. It is expected this is because the multi-wire measures artificially high when there is ice buildup on the leading edge, and because it is more difficult to sufficiently heat the relatively sharp leading edge of the beveled splitter plate to keep it free of ice.

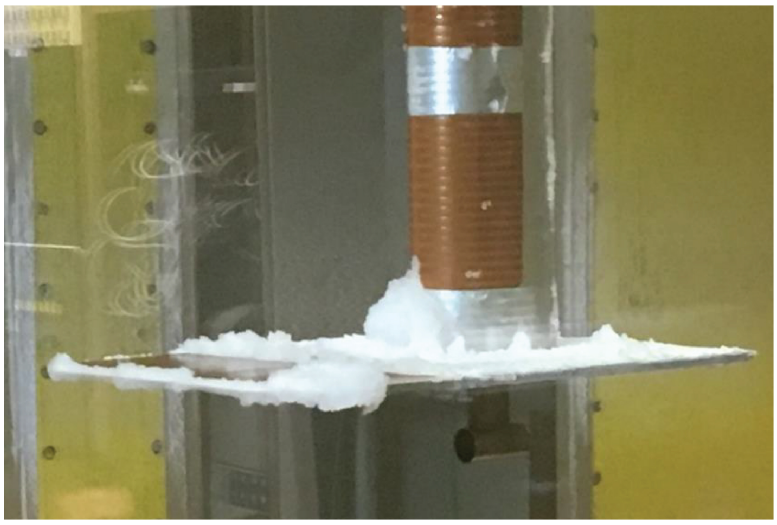

Figure 24.—Observed example of ice buildup on leading edge of beveled leading edge splitter plate in high-impingement-rate condition.

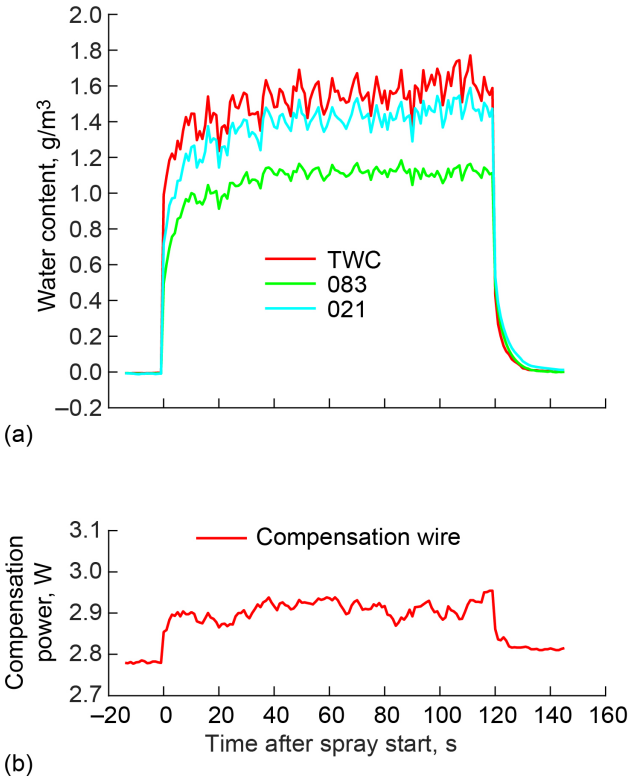

Figure 25.—Multi-wire data traces for high-impingement-rate condition: Airspeed = 250 kn, Standard nozzles, median volumetric diameter = 20 μm. (a) Total water content (TWC), 083, and 021 data with beveled leading edge splitter plate while ice was observed building on leading edge. (b) Compensation wire for beveled leading edge splitter.

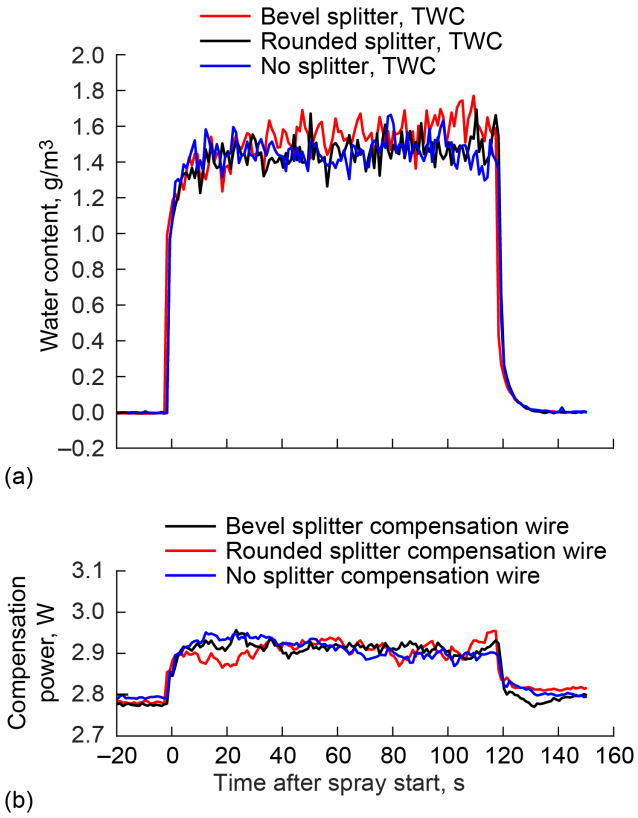

Figure 26.—Multi-wire data traces for high-impingement-rate condition: Airspeed = 250 kn, Standard nozzles, median volumetric diameter = 20 μm. (a) Multi-wire total water content (TWC) data from three configurations for same high-impingement test condition. (b) Compensation wire from all three configurations.

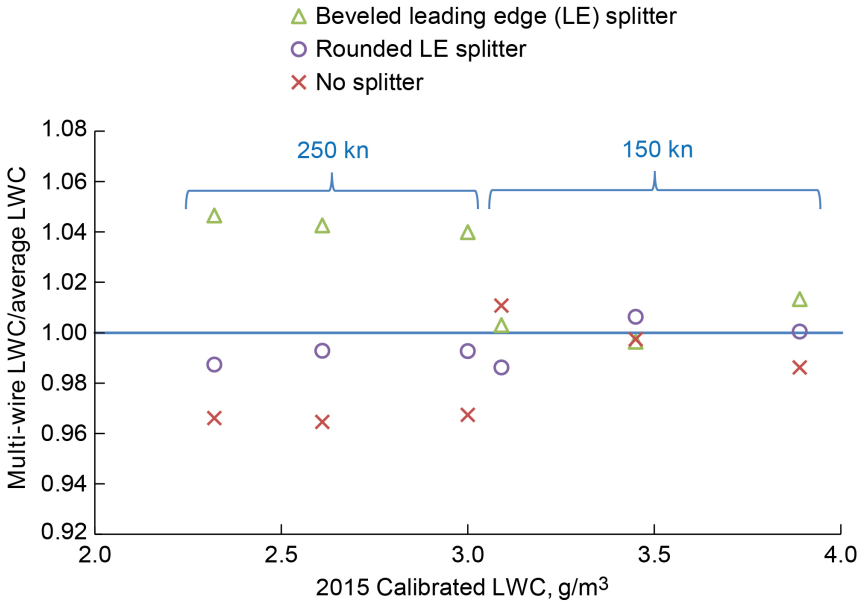

Figure 27.—Measured liquid water content (LWC) from each configuration approaching high-impingement-rate conditions; Mod1 and Standard nozzles were sprayed simultaneously to create high LWC values.

Figure 28.—Ice buildup observed on rounded leading edge splitter plate after failure of one of five cartridge heaters.

The rounded leading edge splitter plate design was chosen in part because it is easier to heat a rounded leading edge than a sharp one. The design featured five cartridge heaters embedded across the leading edge, rather than a Minco heater adhered to the top. These results were largely positive—the leading edge did not suffer from ice buildup the same way that the beveled leading edge splitter did, as indicated by the data in Figure 26. Additionally, even though the leading edge was symmetric, ice buildup mainly occurred on the top of the splitter plate rather than the bottom, presumably due to the blockage from the strut. However, partway through the test day, cartridge heater 4 failed. Because of this, small ice buildup was observed over that heater for high-impingement-rate cases, like that seen in Figure 28. There was little to no discernable impact to the data from this, likely because the heater was off-center and ice buildup still tended to be low.

With no splitter plate, ice buildup still occurred in high-impingement conditions, but not to the same degree as with the beveled leading edge splitter plate. On examining the data traces from the 2016 tests and the 2019 full calibration, there were little to no apparent data trends induced by ice buildup on the strut, as there were with the beveled splitter plate (like in Figure 26). There were occasions of ice shedding observed, which are discussed later.

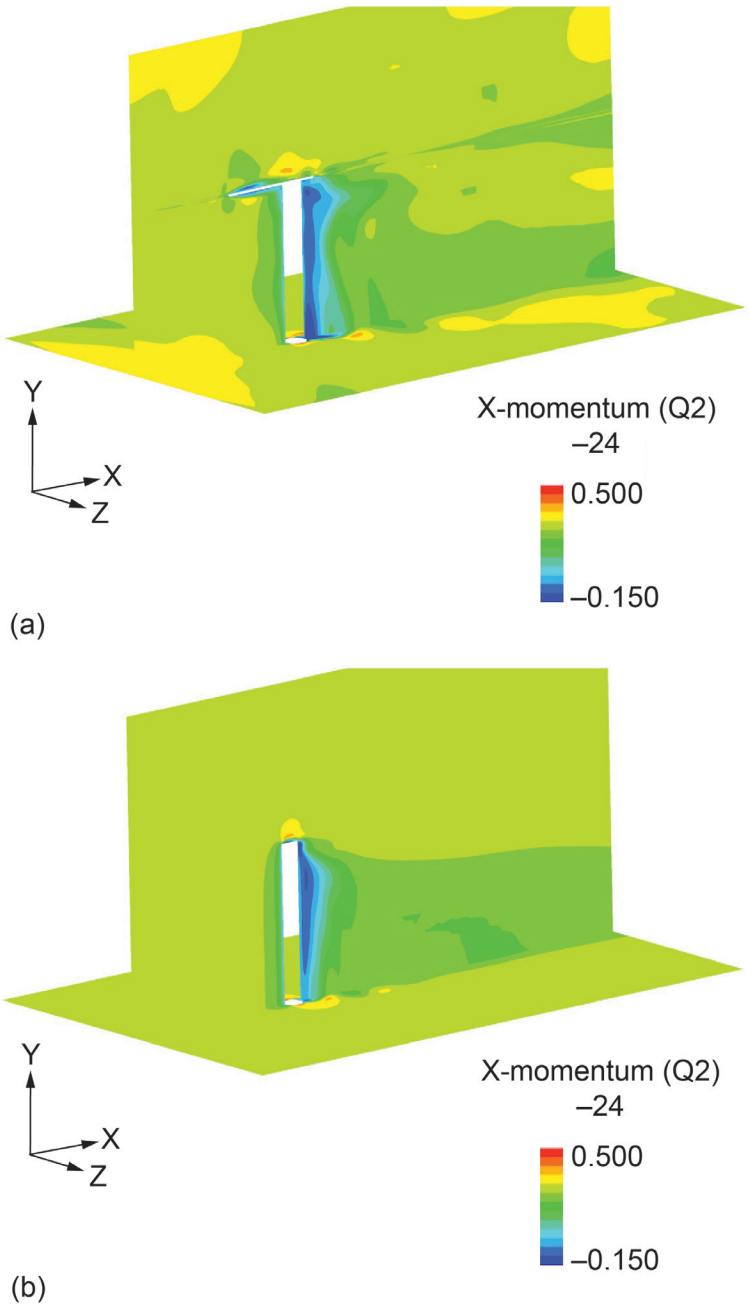

Figure 29.—Computed X-momentum, snapshot. (a) Cylinder mast and beveled splitter plate. (b) Cylinder mast only.

Computational Flow-Field Analyses

Computational flow-field analysis was conducted by Rigby for both the beveled leading edge splitter plate and no splitter plate. This was meant to be a simple effort to observe global effects.
Figure 29 shows respective snapshots of the calculated X-momentum at a vertical plane intersecting the mount with a cylindrical mast (simplified from the actual elliptical geometry), with the beveled splitter plate and with no splitter plate. In these cases, the mount is viewed as if secured to the floor, not the ceiling. The aerodynamic effect of the multi-wire head itself is not considered, since the goal was to determine the impact of the mount without the presence of the multi-wire. Several things may be taken

from the flow-field analyses, but two of the primary observations were that (1) for both configurations, the X-momentum values where the multi-wire sensor head would be installed are very comparable and (2) the splitter plate creates a thin separation bubble upstream of the multi-wire. Since the sharp side of the bevel is on the same side of the plate as the multi-wire, this separation bubble could get larger with facility flow angularity, which has been shown to happen in the IRT (Ref. 19).

Possible Shadowing of Sensing Elements: Sensing Element Power Values

In a 2009 study described in Reference 13, it was suggested that a lack of splitter plate could cause the sensing elements (particularly the compensation wire) to be shadowed from the main airstream, thus reading lower power values and thus biasing the LWC measurements. To investigate this, data comparisons were made of the compensation wire and TWC element power levels, both during the spray (wet) and before the spray (dry). During spray, raw power values were compared across the three configurations for 56 spray conditions (168 sprays, averaged as the LWC values are), and prespray power values (10-s averages) were compared for 50 conditions (i.e., 150 sprays), grouped into like-aerodynamic conditions (V and P_{air}). SEA, Inc., engineers' perception is that power variations of less than 1 percent are likely negligible (Ref. 20). Across the 168 during-spray test points, 94 percent of compensation wire averaged values were within 1 percent of the three-configuration average, and all conditions were within 2 percent of the average. For the same 168 conditions, 61 percent of TWC wire-averaged values were within 1 percent of the three-configuration average, and 94 percent were within 2 percent. Prespray TWC power values were lower in magnitude, but 79 percent of compensation wire power values were within 1 percent of the three-configuration average, as were 51 percent of TWC element power values. Any possible trends that were observed were on the order of 1 to 2 percent variation and do not appear to have impacted the LWC measurement accuracy, with one exception. The beveled splitter configuration showed the highest compensation power values in the Mod1 air pressure sweep, coupled with the lowest TWC power values, which appears to be why its resulting LWC values were lower than the other two and the blade (observed in Figure 22 for LWC values below 1.5 g/m^3). This indicates that targeting higher compensation wire power values will not necessarily lead to more accurate LWC readings. Further scrutiny of power values in the different configurations was not found to have notable impact on data accuracy and will not be discussed further.

Considerations for Flow Steadiness

Calculations were done on the general steadiness of the flow, and simple tuft tests were also performed for each mounting configuration by taping a tuft of yarn on the lower trailing edge of the multi-wire's cylindrical shroud. The tuft showed the greatest fluctuations in the no-splitter configuration. Additionally, the engineers compared within-spray data fluctuations by calculating the standard deviation for LWC fluctuations within each spray condition. The beveled splitter plate configuration most often showed the lowest standard deviations, except in high-impingement conditions (where it is expected the higher fluctuations are due to ice buildup on the leading edge), when it showed the highest standard deviations. However, it must be considered that lower fluctuations in and of themselves do not indicate that the sensor is giving a more accurate representation of the cloud that would exist in the test section, or indicate if the mount is diverting water drops towards or away from the sensor head. Precision is not the same as accuracy, as demonstrated by previous plots where the data had lower fluctuation levels but did not show closer match to blade LWC values—such is the case for the 50 to 150 kn conditions in Figure 20(a) and (b). Hence, flow steadiness was not a driving factor in the decision regarding the multi-wire mount.

Possibility of Ice Shedding

The possibility of ice shedding into the sensor head should receive consideration in all multi-wire testing. Figure 30 shows the multi-wire mounted without a splitter plate, with some ice buildup on the mount leading edge. It was expected that having no splitter plate could reduce shielding for the sensor head from ice that may shed from the mount during the test. Note that ice may also shed from the leading edge of a splitter plate towards the multi-wire head. In the IRT, ice buildup can often be removed from the strut expediently by lowering the tunnel airspeed, thus reducing cooling on the mount and allowing the surface heaters to melt the ice. For the 2019 tests without the splitter plate, the engineers chose to either bring the airspeed to 0 (full stop) or hold around 100 kn so that when ice sheds, it would fall downstream rather than downward into the sensor head.

Over the course of the 2019 full calibration that has been described in this report and for which the multi-wire was mounted without a splitter plate, 558 sprays were recorded with the multi-wire over the span of 7 test days. All the multi-wire data output from the M300 were scanned looking for instances of a power increase measured by the TWC wire larger than 3 W that could not be tied to the cloud turning on. A total of seven instances were observed that were believed to be caused by ice shedding from the mount into the sensor head. Of these, four were during sprays and three were between sprays. Example data traces are shown in Figure 31, which include a minor case and the most major case of spiking that was believed to be caused by ice shedding from the mount. It should be noted that the power and LWC differences shown in Figure 32 from the TWC element are three times larger than for any other recorded instance of shedding ice impinging, that is, this was a singularly bad case. However, in all cases of shedding ice impingement, the power levels of all sensing elements returned to preimpingement values, thus suggesting that any damage to the instrument elements were minor in all of these instances. Visual checks were also performed to see if there was visible damage to the elements. The spray conditions were repeated satisfactorily, and the contaminated data were not used. Health-monitoring checks (described in Ref. 13) were performed daily to ensure dry (spray-off) power values remained consistent for all sensing elements.

No guarantee can be made that ice shedding from the mast will not cause damage to the sensing elements, but this is also true for the splitter plate, which was not without downward ice shed events. The IRT staff have reason to believe ice shed events impacting the sensing elements were more frequent without a splitter plate.

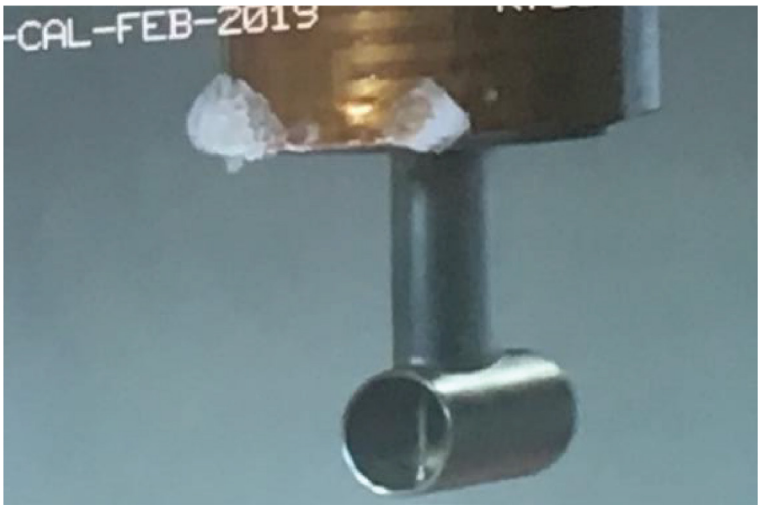

Figure 30.—Ice buildup observed on leading edge of multi-wire strut with no splitter plate.

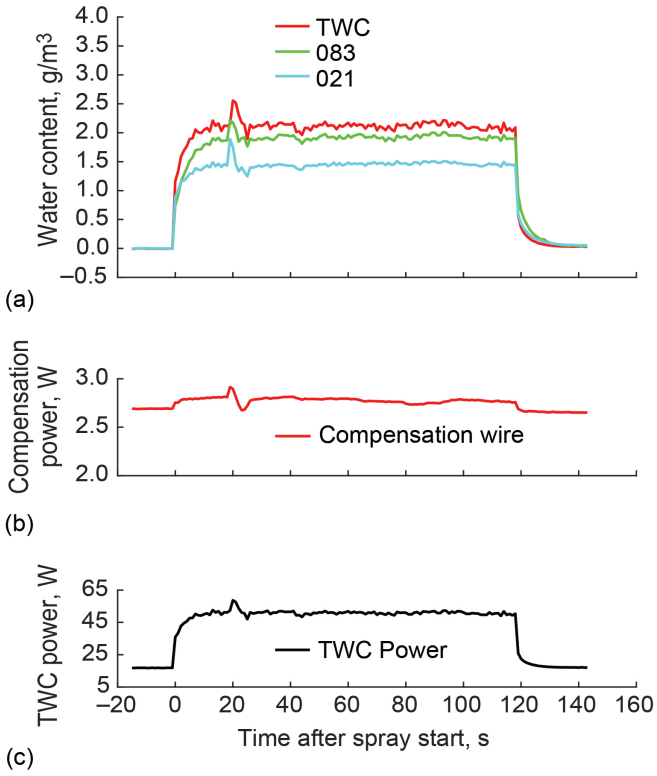

Figure 31.—Example of expected shedding ice impinging on multi-wire elements during spray. Over 558 sprays and 7 multi-wire test days, there were seven instances where ice was believed to have shed into sensor head. Small effect from ice shedding off of strut; Airspeed = 250 kn, median volumetric diameter (MVD) = 24 μm. (a) Water content. (b) Compensation wire power. (c) Total water content (TWC) power.

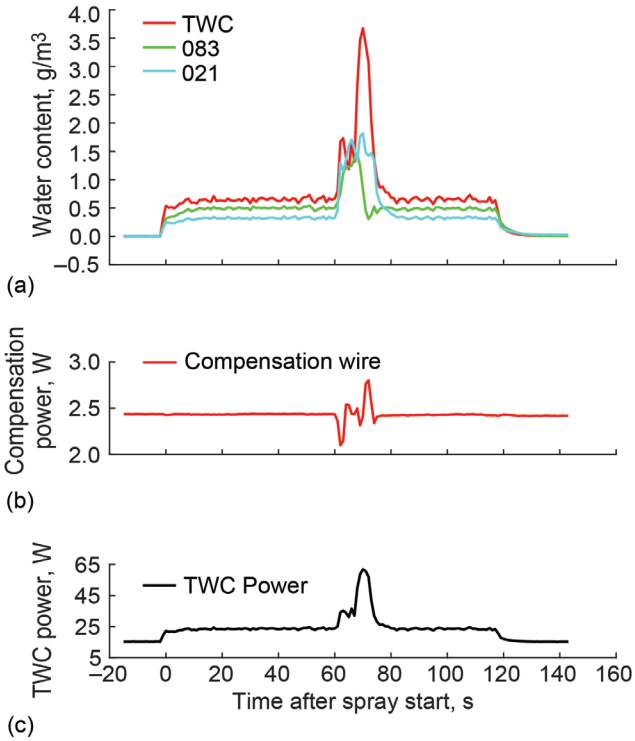

Figure 32.—Example of expected shedding ice impinging on multi-wire elements during spray. Over 558 sprays and seven multi-wire test days, there were seven instances where ice was believed to have shed into sensor head. Large effect from ice shedding off of strut; Airspeed = 200 kn, MVD = 125 μm. Fluctuations in liquid water content and power observed here were three times larger than in any other observed case of ice impingement. (a) Water content. (b) Compensation wire power. (c) TWC power.

Icing Research Tunnel Decision Based on Consideration of Data

It has already been stated in the main text of this report that the IRT staff decided to use the normal mast without a splitter plate for the 2019 full calibration. This decision was primarily because there was no conclusive, discernible improvement to the accuracy of the data by having the splitter plate in place, especially since most of the differences observed were within the overall repeatability capabilities of the multi-wire in the IRT. Secondly, data indicated that removing the splitter plate would allow better measurement of high-impingement-rate conditions; it was more difficult to keep the sharp leading edge of the beveled splitter plate free of ice, and ice buildup caused contamination of the data. After this decision was made, ice shedding events were found to be more frequent than with the splitter plate, but there was no apparent damage to the sensor head or elements. Additional points of consideration have been included in this Appendix, including flow-field calculations, additional contamination of multi-wire data due to shadowing or splashing, steadiness of the readings, none of which were highly conclusive and all of which were considered secondary to data accuracy. To confirm data accuracy with the new configuration, the IRT started the LWC portion of their 2019 full calibration with measurements from the icing blade for conditions below the blade's Ludlam limit. These measurements were presented in the main body of this report and indicated good comparison of data between the blade and the multi-wire without a splitter plate, and IRT staff expect to continue running the multi-wire in this configuration for subsequent interim calibration and check calibrations.

References

1. SAE International: Calibration and Acceptance of Icing Wind Tunnels. ARP5905, 2015.
2. Steen, Laura E., et al.: NASA Glenn Icing Research Tunnel: 2014 and 2015 Cloud Calibration Procedures and Results. NASA/TM—2015-218758, 2015. https://ntrs.nasa.gov
3. Federal Aviation Administration: Atmospheric Icing Conditions. U.S. Code of Federal Regulations, Title 14, Part 25, Appendix C, 2015.
4. Federal Aviation Administration: Supercooled Large Drop Icing Conditions. U.S. Code of Federal Regulations, Title 14, Part 25, Appendix O, 2015.
5. Ide, Robert. F.; and Sheldon, David W.: 2006 Icing Cloud Calibrations of the NASA Glenn Icing Research Tunnel. NASA/TM—2008-215177, 2008. https://ntrs.nasa.gov
6. Federal Aviation Administration: Compliance of Transport Category Airplanes With Certification Requirements for Flight in Icing Conditions. Advisory Circular 25–28, 2014.
7. King-Steen, Laura E.; and Ide, Robert F.: Creating a Bimodal Drop-Size Distribution in the NASA Glenn Icing Research Tunnel. AIAA 2017–4477, 2017.
8. Potapczuk, Mark G.; Tsao, Jen-Ching; and King-Steen, Laura E.: Bimodal SLD Ice Accretion on a NACA 0012 Airfoil Model. AIAA 2017–4478, 2017.
9. Potapczuk, Mark G.; and Tsao, Jen-Ching: Further Examinations of Bimodal SLD Ice Accretion in the NASA Icing Research Tunnel. AIAA 2018–3182, 2018.
10. Potapczuk, Mark G.; and Tsao, Jen-Ching: The Influence of SLD Drop Size Distributions on Ice Accretion in the NASA Icing Research Tunnel. SAE Technical Paper 2019–01–2022, 2019.
11. Potapczuk, Mark G.; and Tsao, Jen-Ching: Bimodal SLD Ice Accretion on Swept NACA 0012 Airfoil Models. AIAA 2020–2814, 2020.
12. Science Engineering Associates, Inc.: WCM–2000. 2016. http://www.scieng.com/pdf/WCM2000User.pdf Accessed Nov. 14, 2020.
13. Steen, Laura-Cheri E.; Ide, Robert F.; and Van Zante, Judith F.: An Assessment of the Icing Blade and the SEA Multi-Element Sensor for Liquid Water Content Calibration of the NASA GRC Icing Research Tunnel. AIAA 2016–4051, 2016.
14. Rigby, David L.; Struk, Peter M.; and Bidwell, Colin: Simulation of Fluid Flow and Collection Efficiency for an SEA Multi-Element Probe. AIAA 2014–2752, 2014.
15. Struk, P.M.: NASA Glenn Research Center, Cleveland, OH, personal communication, 2014.
16. Frost, Walter; Chang, Ho-Pen; and Kimble, Kenneth P.: Particle Trajectory Computer Program for Icing Analysis of Axisymmetric Bodies Final Report. NASA CR– 189134, 1982. https://ntrs.nasa.gov.
17. Box, George E.P.; Hunter, William G.; and Hunter, J. Stuart: Statistics for Experimenters: An Introduction to Design, Data Analysis, and Model Building. Ch. 17, John Wiley & Sons, Inc., New York, NY, 1978.
18. Mandel, John: The Statistical Analysis of Experimental Data. Ch. 4, Dover Publications, Inc., New York, NY, 1964.
19. Rinehart, David A.; and Johnson, Aaron M.: Full Aerothermal Characterization of the 6- by 9-Foot Icing Research Tunnel (2019 Test). NASA/CR—20205005811, 2020. https://ntrs.nasa.gov
20. Bouley, D.: Science Engineering Associates, Inc., Tolland, CT, private communication, 2021.